Int J Earth Sci (Geol Rundsch) (2006) 95: 995–1017
DOI 10.1007/s00531-006-0079-5

ORIGINAL PAPER

J. Escuder-Viruete · A. Pérez-Estaún

Subduction-related *P–T* path for eclogites and garnet glaucophanites from the Samaná Peninsula basement complex, northern Hispaniola

Received: 4 March 2005 / Accepted: 28 January 2006 / Published online: 22 April 2006
© Springer-Verlag 2006

Abstract Eclogite and garnet glaucophanite lenses from the Punta Balandra unit of the Samaná basement complex (northern Hispaniola) preserve information of the early metamorphic and tectonic history of subduction in the Caribbean island-arc and its collision with the North America plate. For this reason, *P–T* paths were reconstructed from the interpretation of meso- and microfabrics, mineral assemblages and chemistry, with the aid of equilibrium phase diagrams calculated for specific bulk compositions in the CKNFMASH system and isopleths for selected solution end-members. The obtained results suggest that the subduction-related prograde path evolved from garnet-free and garnet-bearing lawsonite-blueschist facies, to phengite eclogite facies conditions at $P = 22$–24 kbar and $T = 610$–625°C, with a probable intermediate stage of low-*P* lawsonite eclogite facies. The subsequent retrograde *P–T* path entered the epidote-blueschist (garnet-free) facies and ended within the greenschist facies field, similar to the prograde evolution at low-*P*. Eclogites and garnet glaucophanites formed in a subduction zone in which oceanic lithosphere was subducted WSW/W beneath the Caribbean plate.

Keywords Blueschist · Eclogite · High-*P* metamorphism · Caribbean plate · Equilibrium phase diagrams

Mineral Abbreviations are after Kretz (1983) with the following additions
Phg: Phengite · Fe-Gln: Ferroglaucophane · Mg-Rbk: Magnesio-riebeckite · Na-Amp: Sodic-amphibole · Ca-Amp: Calcic-amphibole · Carb: Carbonates · Cel: Al-celadonite · Fe-Cel: Fe–Al-celadonite · Al–Ae Aug: Aluminous–aegirine augite · Fe-Omp: Ferrian omphacite · Fe–Mg Omp: Ferrian/ferroan-magnesian omphacite · Mg-Omp: Magnesian-omphacite

J. Escuder-Viruete (✉)
Depto. Petrología y Geoquímica, Universidad Complutense, 28040, Madrid, Spain
E-mail: escuder@geo.ucm.es
Tel.: +34-91-3944906/3945014
Fax: +34-91-5442535

A. Pérez-Estaún
Inst. Ciencias Tierra Jaume Almera-CSIC, Lluís Solé Sabarís s/n, 08028, Barcelona, Spain

Introduction

Hispaniola consists of a 250-km wide tectonic collage of fault bounded igneous, metamorphic and sedimentary rocks of the Late Jurassic–Early Cretaceous to Middle Eocene age that formed in an intraoceanic island-arc setting (Fig. 1a; Mann et al. 1991). The Caribbean arc-related rocks are regionally overlain by a cover of Upper Eocene to Pliocene sedimentary rocks that post-date island-arc activity and mainly record the initiation of oblique arc-continent collision between North America and Caribbean plates, as well as active subduction in the southern Hispaniola margin (Mann et al. 1991; Dolan et al. 1998; De Zoeten and Mann 1999; Mann 1999). The association of blueschists, eclogites, mélanges and serpentinites permitted Nagle (1974) to suggest that the high-*P* basement rocks of the Cordillera Septentrional and Samaná Peninsula, in northern Hispaniola, were generated in a subduction zone (Fig. 1b). Mann et al. (1991) grouped these rocks in terranes that originated as fragments of the forearc or accretionary wedge of the arc during NW-directed thrusting of the Caribbean plate onto the North American continental shelf at the Puerto Rico trench (Pindell and Draper 1991; Draper and Nagle 1991; Joyce 1991; De Zoeten and Mann 1999).

Eclogite and blueschist are found in two settings: (1) as tectonically interleaved exotic blocks set in a lower grade serpentinite–matrix mélange (Jagua Clara and Arroyo Sabana mélanges; Draper and Nagle 1991); and (2) as intercalated boudins and lenticular blocks within marble, calc- and micaschist (Samaná basement complex; Joyce 1991; Gonçalves et al. 2000; Catlos and Sorensen 2003). On the southern coast of the Samaná

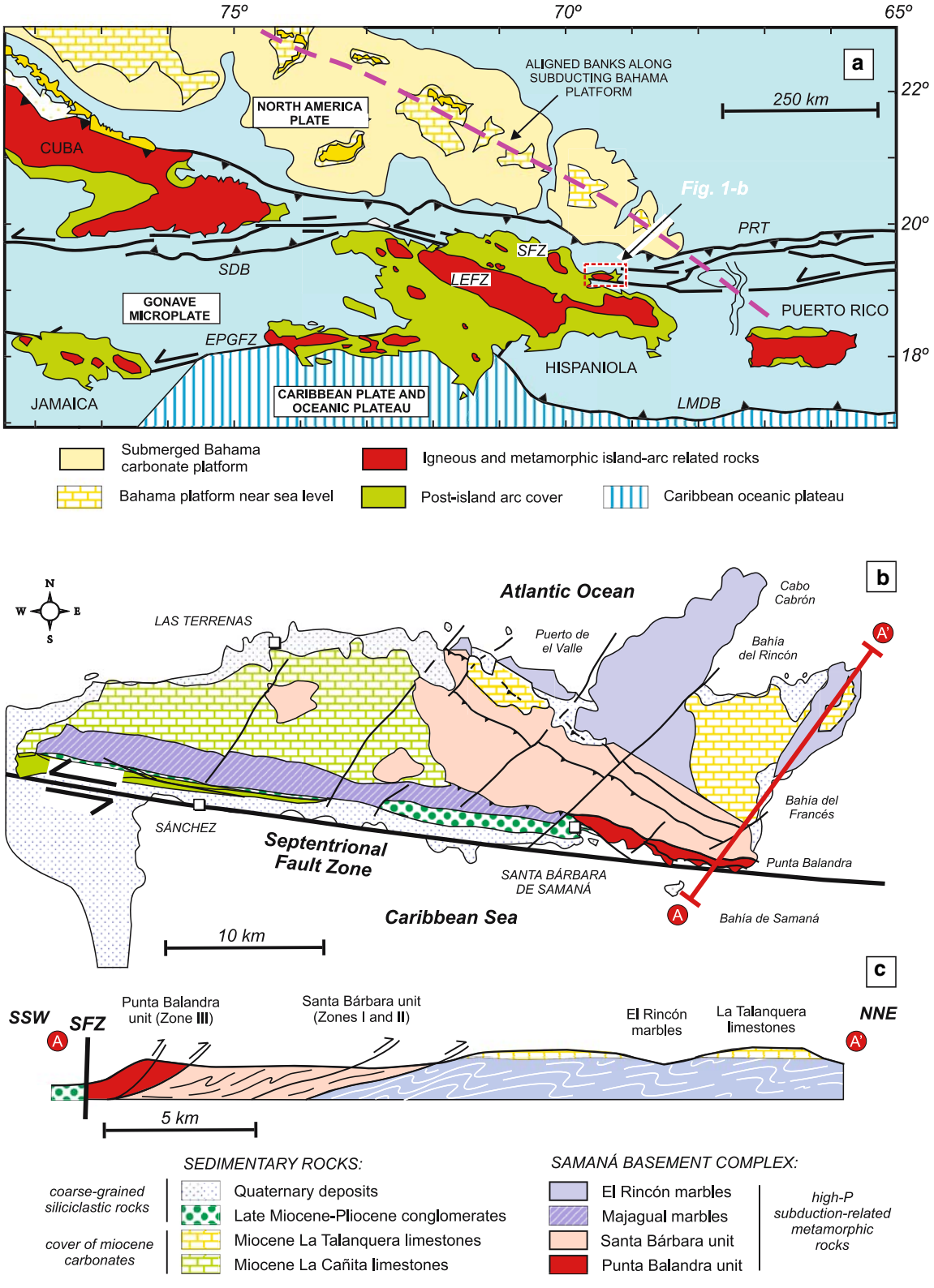

Fig. 1 **a** Map of the northeastern Caribbean plate margin modified from Dolan et al. (1998). *SDB* Santiago deformed belt, *EPGFZ* Enriquillo-Plantain Garden fault zone, *SFZ* Septentrional fault zone, *LEFZ*, La Española fault zone, *PRT* Puerto Rico trench, *LMDB* Los Muertos deformed belt. **b** Geological map of Samaná Peninsula, northern Dominican Republic, modified from Joyce (1991). **c** Synthetic $A-A'$ cross-section of the Samaná Peninsula

Peninsula, a number of eclogite blocks are clean from vegetation and extreme tropical alteration by sea wave action. The surfaces and sections of blocks are almost unique in the Samaná basement complex and provide information on deformation and metamorphism at eclogite and blueschist facies conditions, because blocks are commonly overprinted by a lower grade retrograde and variably metasomatized rim at the other localities.

In this paper, the tectonometamorphic evolution of two types of eclogites and related garnet glaucophanites from the pre-Miocene Samaná basement complex is reconstructed from textures, the sequence of mineral assemblages and mineral chemistries. Equilibrium phase diagrams have been computed for specific bulk compositions in the model system CKNFMASH (CaO–K_2O–Na_2O–FeO–MgO–Al_2O_3–SiO_2–H_2O), using the DOMINO software (De Capitani 1994), an internally consistent thermodynamic database for minerals and appropriate solution models for all major phases occurring in the P–T range of interest. The sequence of mineral assemblages observed in eclogites and hydrated equivalents (retrograde blueschists) shows five metamorphic stages, whose evolution can be interpreted in the equilibrium phase diagrams with the aid of important phase-limiting reactions and P–T conditions estimated by conventional geothermobarometry. Calculations of isopleths for selected mineral end-members are employed to estimate the P–T conditions of some metamorphic stages, to reconstruct metamorphic P–T paths and to illustrate the evolution of mineral composition with respect to changing P and T. The results improve our understanding of the early subduction, collision and exhumation processes within the Caribbean–North America plate boundary zone in Hispaniola.

Geological setting

High-P basement rocks of the Cordillera Septentrional are exposed in three inliers: Puerto Plata, Río San Juan and Samaná basement complexes (Joyce 1991; Pindell and Draper 1991). Mann (1999; and references herein) proposed that all three inliers may have been uplifted by late Neogene restraining bend tectonics along the Septentrional fault zone, which is one of the several strike-slip fault zones separating the Caribbean and North America plates. The geology of the Samaná Peninsula is composed of three elements (Joyce 1991; Fig. 1b, c): (1) a subduction-related metamorphic basement complex whose internal structure consists of a imbricate stack of discrete high-P slabs; (2) an unconformable cover of subhorizontal Miocene limestone formations; and (3) a group of tilted Late Miocene to Pliocene coarse-grained siliciclastic rocks that are both in fault contact and unconformably overlie the metamorphic complex along the south coast. The whole Samaná Peninsula is deformed by sinistral strike-slip and reverse faults associated with the Neogene movement of the Septentrional fault zone.

The Samaná basement complex consists of syntectonically metamorphosed pelitic, carbonate and mafic rocks, alternating in variable relative amounts. Joyce (1991) recognized a sequence of three metamorphic mineral zones, ranging from Lws + Ab-bearing schists in the NE to Omp + Grt-bearing eclogites and Grt-bearing blueschists in the SW. Rocks preserving relict primary structures and recrystallized to Lws + Ab assemblages characterize Zone I (Santa Barbara unit; Gonçalves et al. 2000). A 1–2 km wide narrow intermediate Zone II is defined by Lws + Ab + Gln assemblages in mafic rocks. In the southern side of the peninsula, close to the Septentrional fault zone, Omp + Grt + Phg and Grt + Czo + Gln-bearing assemblages in intercalated mafic boudins and blocks within micaschists and marbles define a Zone III (Punta Balandra unit). The metamorphic sequence represents a metamorphic profile generated during SW-dipping Cretaceous-Eocene subduction (Joyce 1991). However, the increase in grade occurs over a short distance and it can be better explained by the tectonic juxtaposition of units that were metamorphosed at different depths. Minimum P–T conditions achieved were about 13 ± 2 kbar and 450 ± 70°C in the Punta Balandra unit and 7.5 ± 2 kbar and 320 ± 80°C in the Santa Bárbara unit (Gonçalves et al. 2000). Structural data and the pressure gap between them permitted Gonçalves et al. (2000) to deduce that the Punta Balandra unit is thrust over the Santa Bárbara unit and to interpret the metamorphic nappe stack of the Samaná basement complex as a fragment of an accretionary wedge thrust onto the North American continental shelf. Recently, Zack et al. (2004) found a lawsonite eclogite as a pebble on the beach at Punta Balandra, unfortunately without indication of its structural context. These authors calculated the peak-pressure conditions of 16 kbar and 360°C for lawsonite eclogite, indicating a cold subduction of oceanic crust in an accretionary wedge. As suggested by the trace-element geochemistry and the $(\varepsilon_{Nd})_i = +7.2$ value ($t = 86$ Ma), the eclogites studied in this work are Fe- and Ti-rich oceanic metagabbros derived from depleted mantle sources (Escuder-Viruete et al. 2004).

In this study, we are only concerned with metabasites of Zone III, where the effects of at least four episodes of heterogeneous deformation (D1–D4) can be recognized (see also Joyce 1991). In marbles and calc-schists of this zone, compositional layering or lithologic bedding (S0) is subparallel to a WNW/ESE-striking S2 foliation that, in general, dips at a low to moderate angle to the SSW and contains a strong WNW–ESE to W–E oriented L2 mineral and stretching lineation. The non-coaxiality of the D2 deformation is indicated by S–C fabrics, asymmetrical boudinage of the foliation and the asymmetry of winged Grt porphyroblasts. These meso-structures indicate a regionally uniform top-to-the-NE and E shear sense, parallel to the L2. In marble layers, D2 also produced intense isoclinal and intrafolial asymmetric folding with a NE vergence and axes parallel to L2. Oblique grain-shape fabrics in quartz aggregates and S–C

microstructures consistently indicated a top-to-the-NE or E shear sense. An S2 foliation wraps the eclogitic lenses, being able to develop an intense plano-linear (S2–L2) fabric in the rim defined by Phg + Gln + Ep assemblages, in which glaucophane define L2. This epidote-blueschist facies S2 foliation is subparallel or cuts at a high-angle a relict plano-linear (S1–L1) eclogitic fabric present in the core of decimeter- to meter-scale lenses, characterized by omphacite-rich domains that alternate with Grt-rich lenses. The L1 mineral lineation is defined by the elongation of coarse-grained Omp. The S2 foliation is isoclinally folded by WNW/ESE-trending, reclined or recumbent D3 folds and progressively transposed into parallelism with a shallowly SW-dipping S3 that is broadly co-planar with the lower structural boundary of Zone III. In the metapelites, D3 deformation is characterized by the development of retrograde greenschist facies mineral assemblages in S3 planes, high-angle Cal–Chl–Ep veins and normal shear bands that overprint the S2. The S3 foliation was deformed and locally crenulated by open to tight NW/SE to WNW/ESE-trending late D4 folds with a steeply dipping axial-plane, amplitudes of tens of meters and wavelengths of the order of 100 m. D4 subvertical folding is related to the formation of high-angle sinistral shear zones oriented parallel to the S4 axial-plane fabric.

Equilibrium phase diagrams

Equilibrium phase diagrams for eclogite samples from the Samaná basement complex were calculated with the computer code THERIAK-DOMINO (De Capitani 1994) (http://www.therion.minpet.unibas.ch/minpet/groups/theruser.html). DOMINO calculates equilibrium phase assemblages by minimization of the total Gibbs free energy (ΔG) in a given P–T space. The extent and absolute positions of the resulting different stability fields are dependent on the solution models for each multicomponent phase and the bulk composition given in the input. The calculations take into account all minerals in the thermodynamic database and need solution models covering the entire compositional range of each multicomponent phase. Table 1 includes details of the solution models used for the calculation of equilibrium phase diagrams. The thermodynamic database is an updated version of the internally consistent database of Berman (1988), including properties of pumpellyite and glaucophane of Evans (1990), and pargasite and ferropargasite of Mäder and Berman (1992).

The main input of DOMINO consists of a simplified bulk composition in the CKNFMASH model system estimated from modal (volume) proportions from thin sections and microprobe analyses, following Meyre et al. (1997). Minor components such as Mn and Ti are not taken into account because these elements are not included in the solution models. The pure phases of quartz and H_2O are added in excess to ensure their presence in all computations, due to the fact that Qtz and several major hydrous phases (Chl, Lws, Ep/Clz, Amp and Phg) form part of all metamorphic stages, including the eclogitic peak (see below). A relatively high a_{H_2O} is consistent with the phase relations and water contents in progressively dehydrated subducting basalts, experimentally obtained by Schmidt and Poli (1998). The input used in this work is a combination of adjacent phase rim compositions record of the eclogitic thermal peak, taking into account possible changes in their compositions by exchange or net-transfer retrograde reactions. We thus compute the local equilibrium of an observed assemblage restricted to a small closed system. Estimations are only valid within a restricted P–T range, because all of the equilibrium phase diagrams are calculated for a fixed bulk chemistry. Processes that affect the bulk composition, as transport-controlled garnet growth, disequilibrium, influx or outflux of fluids (see Konrad-Schmolke et al. 2005 for a review), were not entirely modeled.

Table 1 Solution models used for the calculation of equilibrium phase diagrams

Phase	Solution model	Reference
Omp	Ternary (Jd, Di, Hd), non-ideal	Meyre et al. (1997)
Grt	Ternary (Grs, Alm, Prp), non-ideal	Berman (1990)
Fsp	Ternary (Ab, Kfs, An), non-ideal	Fuhrman and Lindsley (1988)
Wm	Binary (Pg, Ms), non-ideal	Chatterjee and Froese (1975)
Phg	Ternary (Ms, Cel, Fe-Cel), non-ideal	Massonne and Szpurka (1997)
Ca–Na-Amp	Binary (Parg, Fe-Parg), ideal	This study
Chl	Binary (clinochl, daph), ideal	This study
Ep	Binary (Czo, Ep), ideal	This study

The main problem in modeling mafic rocks is the lack of thermodynamic data for amphibole of barroisite to glaucophane compositions. Barroisitic amphiboles cannot be satisfactorily modeled because of the still not well known thermodynamic mixing properties between Na-, Ca- and Na–Ca amphiboles. Although mixing models have been proposed (Willner 2005), in this study, the thermodynamic data for the glaucophane end-member (Evans 1990) were added to the database and the Na–Ca-Amp was modeled using an ideal binary solution model with the end-members pargasite and ferropargasite (Mäder et al. 1994; Meyre et al. 1997). As barroisitic compositions have not been analyzed in the studied samples, the position and extent of the excluding stability fields of this Na–Ca-Amp model allow some qualitative estimates to be made for the retrograde P–T evolution of eclogites.

Textures and mineralogy

In the Punta Balandra unit, there are two main textural types of eclogite: dark green, weak or non-foliated, type

I granoblastic eclogite; and light green, intensely foliated, type II blastomylonitic eclogite. Both types contain Grt + Omp assemblages that were minimally affected by the retrograde hydration, lack plagioclase and are true eclogites (after Carswell 1990). The recrystallization of type I and II eclogites to a rim of coarse-grained hydrous-mineral rich "glaucophanite" (Fig. 2a) was related to fluid influx along D2 shear zones and S2 foliation planes that wrap around the decimeter- to meter-scale lenses and preserve diverse mineral assemblages and eclogite facies foliations. Individual hydrous shear zones have complex internal structural and metamorphic relationships: pods of partially to pervasively recrystallized eclogite are enveloped by Gln + Chl + Ep + Phg-rich blastomylonites, commonly characterized by a strong L2 mineral and stretching lineation. In D2 low strain domains, retrograde minerals are commonly randomly oriented and patchily developed. Eclogite facies assemblages persist in these domains, presumably owing to the irregularities in strain and/or restricted fluid penetration.

Type I eclogite

Garnet-rich seams and laminae alternate with Omp-rich domains to define a weak S1 granoblastic foliation in type I eclogites. Phg occurs as 2–6 mm long lepidoblasts in stable contact with Grt and Omp (Fig. 2c, d). Qtz is modally less significant, and Ttn and Rut modally more abundant than in type II eclogite. Both large idioblastic Omp laths and aggregates (Cpx-III) have an irregular optical zoning and may contain Gln and Rut inclusions. Matrix Rut is commonly mantled by Ttn and has rare inclusions of Gln. Idioblastic Grt grains are 3–8 mm in diameter and have an internal Mn-rich, inclusion-poor core (not present in all the grains) and an external inclusion-rich zone enclosed by an inclusion-poor or free rim (Fig. 2c, d). Inclusions of Lws pseudomorphs, Ep, Pg, Qtz, Ab, Phg and Chl, are randomly oriented. Type I eclogite is replaced along fractures, veins and patches by a violet–blue aggregate that consists of retrograde Gln, Ep, Phg and Carb, indicating that some of the high-*P* deformation was brittle and accompanied by high fluid activity. In the rim of the lenses, S1 is boudinaged and cut at low angle by a strong S2 mylonitic foliation defined by a preferred mineral orientation of Ep, Phg and Gln/Mg-Rbk that envelope Grt + Omp relic assemblages. In S2 planes, Grt porphyroclasts are replaced in pressure shadows and pull-aparts by Gln + Phg + Ep/Czo ± Carb ± Chl assemblages, and Omp is plastically deformed and fractured. Large euhedral Gln laths parallel to L2 are zoned and have a core-rim compositional range from colorless or pale violet Gln to violet Fe-rich Gln and blue Mg-Rbk (Fig. 2f). Some Gln nematoblasts have relic cores of Act to Mg-Hbl (see below) or include xenoblastic Omp (Fig. 2j). Matrix Gln is locally rimmed by a green Act. Omp and Grt grains are replaced by late- to post-S2 Ab poikiloblasts and Chl + Phg aggregates.

Type II eclogite

Type II blastomylonitic eclogite with minimal secondary recrystallization contains large grains of idioblastic Grt (2–10 mm in diameter), enveloped by a coarse-grained granoblastic S1 eclogitic foliation defined by Omp, Phg, Qtz and Rut, with or without Gln, Ep, Ap and Ttn (Fig. 2e). An L1 mineral lineation is defined by the elongation of Omp nematoblasts and Qtz ribbons. Matrix Omp (Cpx-III) is subidioblastic and nearly colorless. Grt grains preserve complex inclusions patterns (Fig. 2h). Commonly, an inclusion-rich core contains random or aligned inclusions trails that define a sigmoidal to spiral internal foliation continuous with the external S1 foliation, which is made up of Lws, Pg, Ep/Clz, Cpx-I/Cpx II, Chl, Ttn, Rut and Qtz. In many cases, Lws inclusions are replaced by Pg + Ep rhomboidal pseudomorphs. Lws and Cpx-I/Cpx-II inclusions in Grt are never found in direct contact. Grt core is surrounded by a comparatively inclusion-poor rim that forms one-third or less of the grain (Fig. 2h). Partial overgrowth on the inclusion-poor domain is continuous with the enveloping external S1 foliation, consistent with the syn-D1 growth. Some large Grt grains (0.8–1 cm in diameter) display optically distinguishable Grs- and Sps-rich (pre-S1 inclusion-free) cores not present in smaller grains of the same rock. Relatively low strain D2 zones and boudin rims are characterized by Grt porphyroclasts partially replaced in syn-D2 pull-aparts by Gln + Phg ± Carb aggregates (Fig. 2e). Omp grains are intensely affected by cracks subperpendicular to the L2, which are filled by Gln + Phg + Ep assemblages. Omp also forms aggregates of dynamically recrystallized small grains (Fig. 2e). In D2 shear zones, Grt and Omp porphyroclasts are surrounded by bands rich in Gln, Ep, Phg and Carb that define a S–C mylonitic S2 fabric, frequently subparallel to S1. Large Gln laths parallel to L2 are boudinaged with Phg + Carb filling the open pull-aparts. These microtextures, together with the change in amphibole and phengite chemistry (see below), are consistent with the retrograde nature of the S2 fabric in these bands. In addition, Ttn encloses Rut grains and Grt is replaced in the cracks and rims by late- and post-S2 Chl + Phg + Clz + Carb.

Glaucophanite

Glaucophanite and garnet glaucophanite are pervasively recrystallized type I and II eclogites in pods as well as the hydrous D2 shear zones. Coarse-grained, random zoned Gln, Ep/Clz, Phg, Rut and Carb are interpreted to be in textural equilibrium. In such rocks, however, Omp is only present as inclusions in subidio to xenoblastic Grt, being Cpx-II in the core and Cpx-III in the rim.

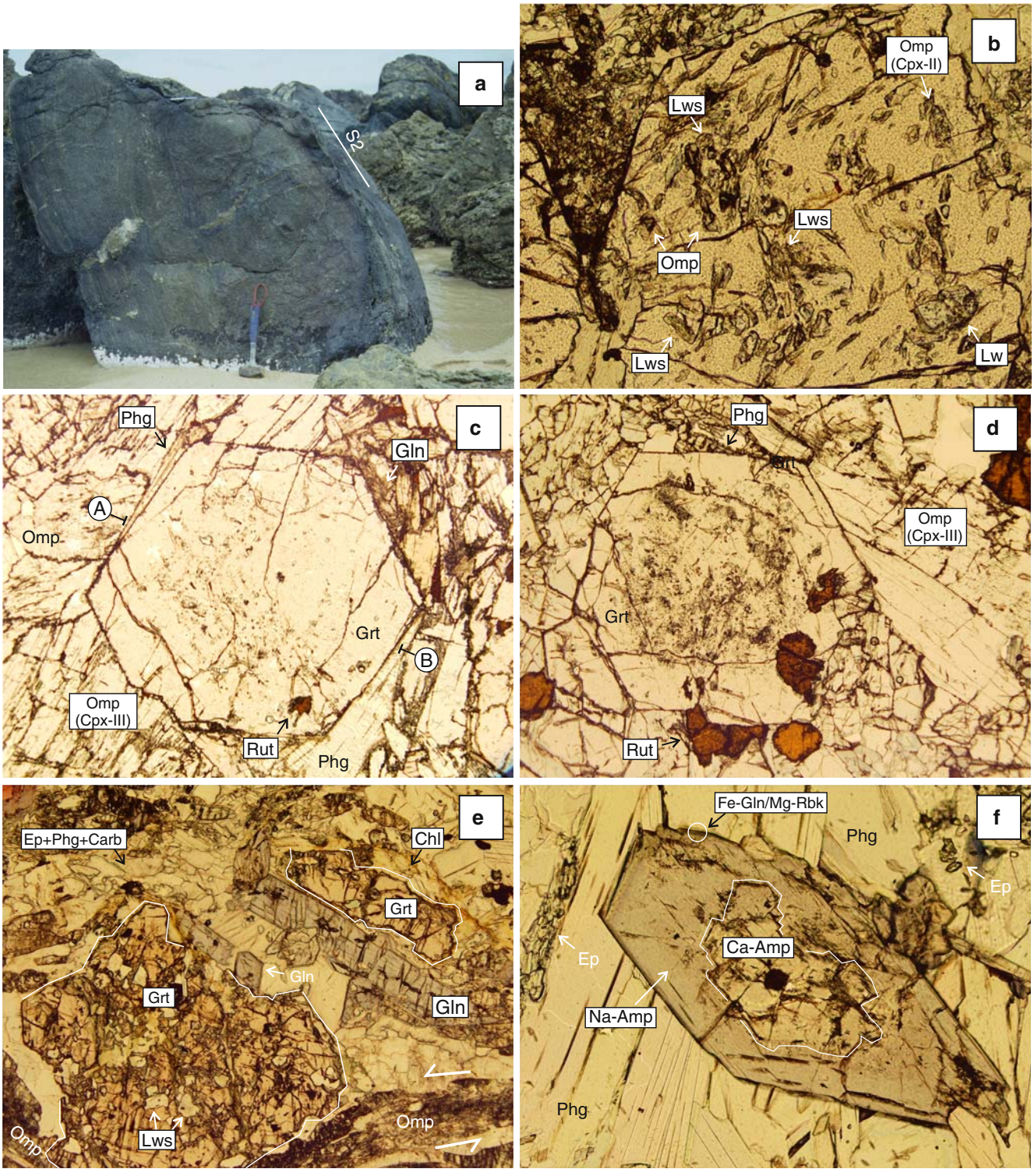

Fig. 2 **a** Type II eclogite boudin with a S1 granoblastic fabric surounded by an envelope of foliated (S2) blueschist. S2 cuts at low angle the boudinaged eclogitic S1 fabric. Puerto Viejo sector, Punta Balandra unit. **b** Grt porphyroblast with a S1 folded foliation defined by Omp + Lws + Qtz + Phg + Rut inclusions of metamorphic stages 1 and 2. J71 sample of type II eclogite. Width of field, 4 mm. **c** Nematoblastic S1 fabric defined by the eclogitic stage 3 assemblage Grt + Omp + Phg + Qtz + Rut in type I eclogite (J74 sample). *A–B* marks the location of the compositional profiles given in Figs. 4 and 7. Width of field, 4 mm. **d** Eclogitic stage 3 in the same J74 sample. Note the inclusion-rich internal zone of Grt. Width of field, 4 mm. **e** Deformation and partial replacement of stage 3 assemblage during stage 4, J78 sample of type II eclogite. Garnet pull-aparts are filled with a large Gln nematoblast and Phg + Ep + Carb. Note in the lower right Omp forms aggregates of recrystallized small grains parallel to the mylonitic S2 foliation. Width of field, 6 mm. **f** Stage 4 retrograde aggregate composed of Na-Amp + Phg + Ep ± Carb with a relic of Ca-Amp in the J122 sample of type I eclogite. Width of field, 1 mm.

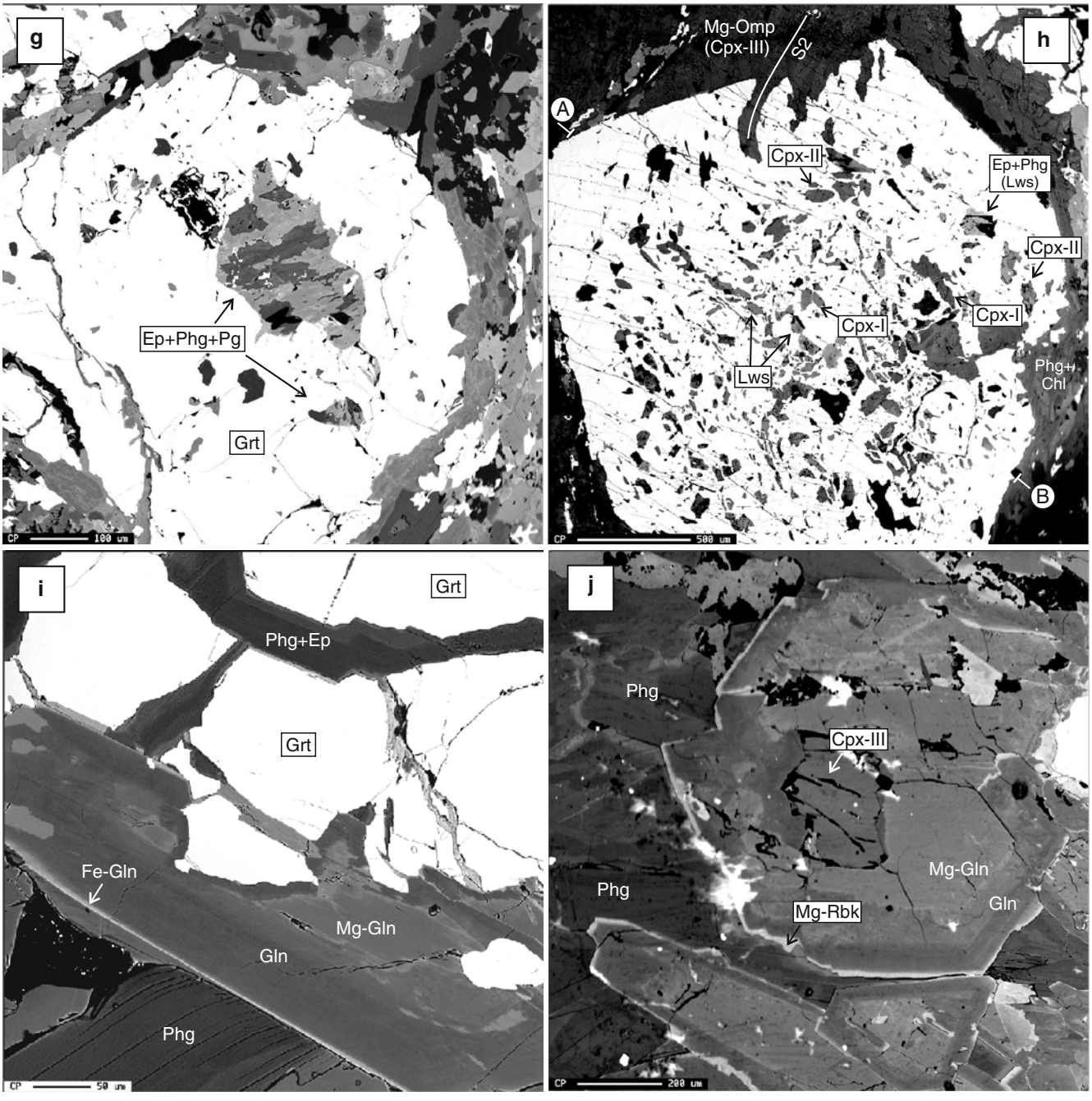

Fig. 2 (Contd.) *Back-scattered electron images of microtextures.* **g** Inclusion of Lws in Grt, pseudomorphosed by Pg + Ep + Qtz ± Phg aggregates in type I eclogite. **h** Grt porphyroblast in type II eclogite with inclusions that define a folded internal S1 foliation, continuous with the external S2 foliation defined by elongated Omp nematoblasts. The inclusions are Lws and Cpx-I (Ae-Aug) in the core and Lws pseudomorphs of Pg + Ep ± Phg and Cpx-II (Omp) in the rim. Matrix Cpx-III is Mg-Omp to Omp. Note the Grt replacement in the rim by Phg + Chl retrograde aggregates. **i** Garnet fractures and pull-aparts have been filled with Phg + Ep (*upper*) and a large zoned Gln nematoblast (*lower*) during retrograde stage 4. **j** Stage 4 retrograde aggregate composed of Na-Amp and Phg in the J122 sample of type I eclogite with a relic of stage 3 Mg-Omp (Cpx-III)

This mineral chemistry is consistent with the Omp inclusions having formed under similar metamorphic conditions as type I and II eclogites, with the Gln-rich matrix being part of a retrograde assemblage developed early in the hydration event. In the D2 shear zones, intensely foliated retrograde assemblages are formed with Na- and Ca-Amp, Fe-rich Ep, Clz, Phg and Carb, with or without Ttn and Ab. In the S2 foliated matrix, violet Gln is intergrown with blue Fe-Gln/Mg-Rbk and pale green Act. Aggregates of Chl + Phg ± Ab ± Carb form pseudomorphs after Gr and Omp is replaced by Gln/Mg-Rbk, Ep/Clz and Ab. Albite form late-S2 porphyroblasts with curved inclusion trails of Gln, Qtz, Ep and Phg.

Interpreted sequence of mineral assemblages

The mineral assemblages described above can be used to establish a sequence of metamorphic stages, whose temporal evolution is interpreted with the help of important facies-limiting reactions in the computed equilibrium phase diagrams. In the eclogites and glaucophanites five different metamorphic stages can be defined, which are shown in Fig. 3 and described below.

Stages 0 and 1 minerals occur as relicts mainly preserved included in the central parts of garnet porphyroblasts. *Stage 0* is characterized by the mineral assemblage Act/Mg-Hbl + Chl + Ep/Czo + Phg + Qtz ± Ab ± Pg ± Carb ± Ttn in type I eclogites, which belongs to the greenschist transitional to albite-epidote amphibolite facies (Evans 1990). As evidenced by the occurrence of relic Si-poor Ca-Amp (Al^{VI} and Ti-rich Act and Mg-Hbl), some blocks of type I eclogite had already been subjected to high-*T*/low-*P* metamorphism on the ocean floor. *Stage 1* is represented by the assemblage Lws + Qtz + Chl ± Pg ± Cpx-I ± Phg ± Rut in type II eclogites, which belongs to the high-*P* lawsonite-blueschists facies, above the reaction Ab → jadeitic Cpx + Qtz (Holland 1983). These minerals commonly define an internal S1, crenulated to varying degrees by the D2 deformation. Garnet glaucophanites have the probably stage 0 assemblage Chl + Phg ± Act + Qtz. *Stage 2* is characterized by the assemblage Ep + Pg + Phg + Qtz + Rut ± Chl ± Gln ± Mn-rich Grt in type I eclogite and Ep + Pg + Phg + Cpx-I/Cpx-II + Qtz + Rut ± Chl ± Ttn ± Mn-rich Grt in type II eclogite. The stage 2 assemblages occur as inclusions in the outer rim of garnets and are characteristic of the garnet-bearing epidote-blueschists facies (*T* > 400–450°C; Evans 1990). *Stage 3* is represented by the assemblage Grt + Omp (Cpx-II/Cpx-III) + Phg ± Qtz + Rut ± Pg (without Lws) in both type I and II eclogites, which belong to the phengite-bearing eclogite facies and define a blastomylonitic S1/early syn-S2 foliation in type II eclogite. *Stage 4* in type I and II eclogites is characterized by the hydrous assemblage Na-Amp + Ep/Czo + Phg + Carb ± Qtz ± Chl ± Rut + Ttn, which overprints the stage 3 eclogite facies assemblage and defines a well-developed S2 retrograde mylonitic foliation. These mineral assemblages are characteristic for the high-*T* part of the garnet-free epidote-blueschist facies (*T* < 400–450°C; Evans 1990). The core-to-rim composition of amphibole grown during stage 4 also suggests its retrograde nature (see below). In the garnet glaucophanites, the corresponding assemblage is Na-Amp + Ca-Amp + Ep/Czo + Phg + Ttn, representing the lower temperature part of the epidote-blueschist facies. In places, Ca-rich phases seem to disappear, resulting in rocks almost entirely composed of glaucophane with minor amounts of Phg and Ttn. *Stage 5* involves recrystallization of the stage 4 minerals and the breakdown of Grt to Chl ± Ep/Czo and omphacite to Ab ± Ep/Clz in type I and II eclogites. Gln is replaced by Act and Rut is mantled or totally pseudomorphosed by Ttn.

In summary, the studied rocks have thus undergone a prograde metamorphic evolution from the lawsonite-blueschist (stage 1) through garnet-bearing epidote-blueschist (stage 2) to the eclogite facies (stage 3), with a subsequent retrograde evolution to the garnet-free epidote-blueschist facies (stage 4) and greenschist facies

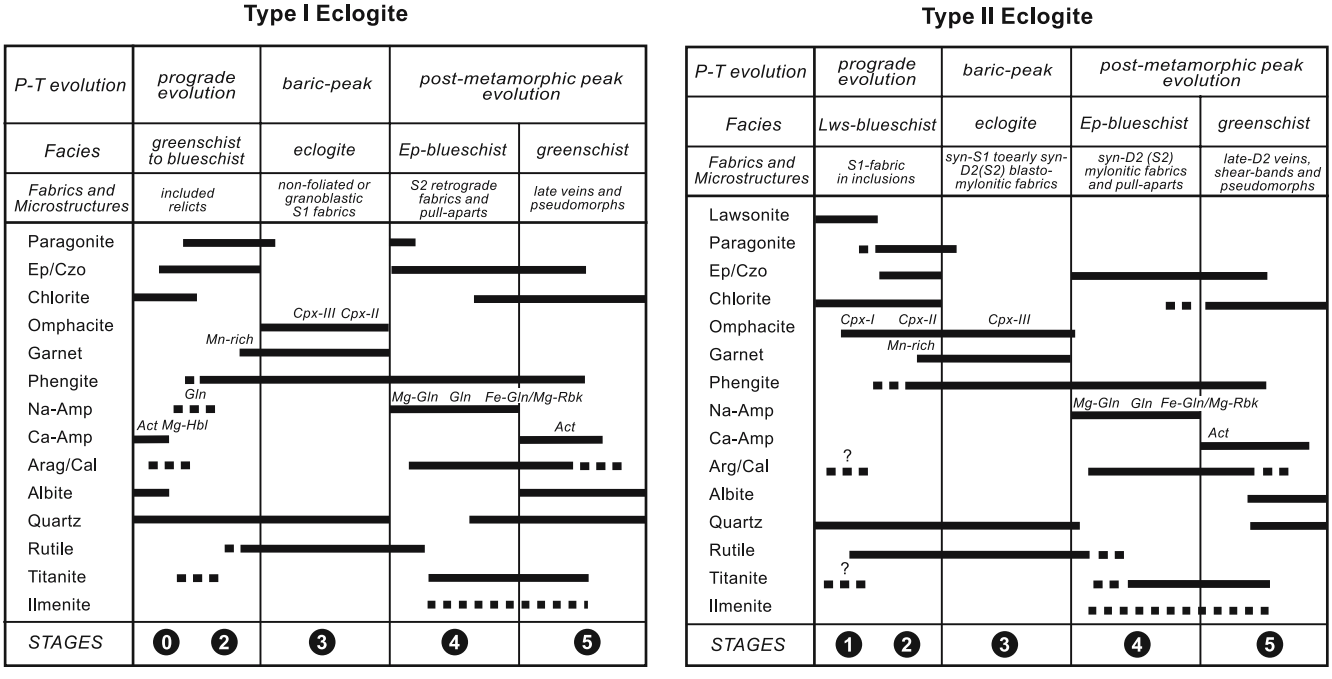

Fig. 3 Summary of the observed relationships between mineral growth and fabrics in the different stages of metamorphic evolution. Cpx-I, aegirine augite; Cpx-II, omphacite; Cpx-III, Mg-rich omphacite

(stage 5). The small difference observed in the two parallel sets of mineral assemblages for type I and II eclogites is probably due to differences in bulk-rock chemistry, with the protoliths of the first slightly more FeO and Al_2O_3-rich and CaO-poor.

Mineral chemistry

Chemical compositions of minerals from six selected samples representative of type I (J74 and J122) and II (J71 and J78) eclogite and garnet glaucophanite (J123 and J125) were studied in detail. Chemical analyses were performed on the JEOL Superprobe JXA-8900M W/ED combined microanalyzer at the Universidad Complutense of Madrid. Analytical conditions were a 15 kV accelerating potential, 20 nA specimen current and 1 μm beam diameter. In each sample, Grt porphyroblasts with the largest diameter (between 2.0 and 4.5 mm) were analyzed along rim-core-rim traverses at regular intervals (40–75 μm depending on the size). Matrix minerals are often zoned and rim-core-rim traverses with 5–15 evenly spaced spot analyses were performed in Omp, Amp and Phg. Other matrix minerals were analyzed at 3–5 spots per grain. Representative mineral analyses, particularly those used in the thermobarometric calculations, are given in Tables 2, 3, 4, 5 and 6. For selected Grt and Amp grains, Fe, Mn, Mg, Ca and Na X-ray mappings were carried out using the same probe. The complete data-set for all samples used in this study can be obtained from the authors upon request.

Garnet

Along the textural zoning, type I eclogites display a symmetric outward decrease of X_{Sps} and X_{Grs} (from 0.20 to 0.04 and from 0.35 to 0.18, respectively), an increase in X_{Alm} and X_{Prp} (from 0.44 to 0.58 and from 0.04 to 0.28, respectively) and a decrease in X_{Fe} [= Fe/(Fe + Mg), from 0.92 to 0.62] (Fig. 4). These trends are typical of prograde growth zoning (Spear 1993) from metamorphic stages 2 to 3. In grains for which compositional maps were done (Fig. 5a), contours of Fe, Mn, Mg and Ca show near-euhedral shapes, which represent traces of the successive growth surfaces during stages 2–3. In detail, some Grt grains are characterized by a radiating or cross-pattern in the Mg and Fe (not in Ca and Mn) that post-date the garnet core and predate the inclusion-poor or free outermost rim. The overall zoning patterns appear to be unaltered by post-growth diffusion, except in the local embayments at the Grt rim (Fig. 5a), where the chemical trends are reversed in the

Table 2 Representative analyses of garnet from eclogites and garnet glaucophanites

Lithology	Type I	Type I	Type I	Type I	Type II	Type II	Type II	Type II	Type II	gg	gg	gg
Sample	J-74	J-74B	J-122	J-122	J-78	J-78	J-71	J-71	J-71	J-123	J-123	J-125
Grain	GRT-2	GRT-1	GRT-1	GRT-1	GRT-4	GRT-4	GRT-1	GRT-1	GRT-1	GRT-1	GRT-1	GRT-3
Analyses	115-r	59-rt	26-r	18-c	101-r	148-rt	13-c	11-i	12-r	72-ig	6-ig-c	52-r
Stage	3	3	3	2	3	3	2	2	3	3	3	3
SiO_2	38.91	38.64	38.31	38.03	38.56	37.32	37.84	37.62	39.35	37.87	38.94	38.29
TiO_2	0.06	0.04	0.01	0.11	0.04	0.00	0.13	0.14	0.04	0.15	0.16	0.18
Al_2O_3	22.07	22.51	21.92	21.61	21.84	20.91	21.42	21.64	21.63	21.96	21.73	21.92
Cr_2O_3	0.00	0.01	0.01	0.00	0.03	0.00	0.00	0.07	0.06	0.02	0.15	0.04
FeO	22.33	24.94	23.97	26.88	24.93	26.82	27.14	27.43	28.31	25.50	24.38	25.39
MgO	7.62	6.76	5.84	2.21	3.11	3.22	0.94	1.36	2.87	3.11	2.82	3.26
MnO	0.47	0.42	0.17	0.28	0.09	0.30	1.20	0.45	0.20	0.73	1.57	0.46
CaO	7.97	7.31	9.19	11.33	11.47	9.86	10.80	10.72	9.22	10.24	10.20	10.60
Na_2O	0.03	0.04	0.01	0.01	0.04	0.04	0.00	0.05	0.02	0.02	0.03	0.06
K_2O	0.00	0.00	0.00	0.00	0.00	0.02	0.00	0.00	0.01	0.00	0.00	0.00
Total	99.46	100.67	99.43	100.45	100.10	98.48	99.47	99.48	101.72	99.61	99.98	100.20
Si	5.989	5.933	5.964	5.981	6.021	5.983	6.037	5.993	6.088	5.965	6.085	5.985
Al	4.003	4.074	4.022	4.005	4.019	3.950	4.027	4.062	3.945	4.076	4.002	4.037
Ti	0.007	0.005	0.001	0.013	0.005	0.000	0.016	0.017	0.005	0.018	0.019	0.021
Cr	0.000	0.001	0.002	0.000	0.004	0.000	0.001	0.008	0.007	0.003	0.018	0.005
Fe	2.874	3.202	3.121	3.536	3.255	3.596	3.622	3.653	3.664	3.358	3.186	3.318
Mg	1.749	1.548	1.356	0.519	0.725	0.770	0.225	0.323	0.661	0.731	0.657	0.759
Mn	0.061	0.055	0.022	0.037	0.011	0.041	0.162	0.061	0.026	0.097	0.207	0.061
Ca	1.314	1.202	1.534	1.909	1.918	1.694	1.845	1.829	1.529	1.727	1.708	1.775
Na	0.010	0.013	0.003	0.003	0.011	0.011	0.000	0.015	0.007	0.006	0.008	0.019
K	0.000	0.000	0.000	0.000	0.000	0.004	0.000	0.000	0.002	0.000	0.000	0.000
X_{Fe}	0.62	0.67	0.70	0.87	0.82	0.82	0.94	0.92	0.85	0.82	0.83	0.81
X_{Alm}	0.48	0.53	0.52	0.59	0.55	0.59	0.62	0.62	0.62	0.57	0.55	0.56
X_{Prp}	0.29	0.26	0.22	0.09	0.12	0.13	0.04	0.06	0.11	0.12	0.11	0.13
X_{Sps}	0.01	0.01	0.00	0.01	0.00	0.01	0.03	0.01	0.00	0.02	0.04	0.01
X_{Grs}	0.22	0.20	0.25	0.32	0.32	0.28	0.32	0.31	0.26	0.29	0.30	0.30

Normalization scheme to 24 O. *gg* garnet glaucophanite. Garnet analyses: *c* core, *i* intermediate, *r* rim, *rt* rim touching clinopyroxene, *ig* garnet adjacent to clinopyroxene inclusion

Table 3 Representative analyses of clinopyroxene from eclogites and garnet glaucophanites

Lithology	Type I	Type I	Type I	Type I	Type I	Type II	Type II	Type II	Type II	Type II	gg	gg
Sample	J-74	J-74	J-122	J-122	J-122	J-78	J-78	J-78	J-78	J-78	J-123	J-123
Analyses	27-r	1-r	124	125	2	43-r	160-i	32-i	34-i	153-r	63-i	88-i
Stage	3	3	3	3	3	3	2	2	1	3	3	3
	MO	MO	MO	OM	MO	MO	OM	OM	AA	OM	MO	MO
SiO_2	55.98	56.51	55.73	54.51	55.78	56.01	54.44	54.93	54.09	55.77	55.37	55.50
Al_2O_3	10.71	11.10	11.96	12.02	12.05	11.42	6.50	8.47	5.50	11.32	9.28	8.15
FeO	3.41	2.94	3.58	3.83	3.55	4.91	10.92	6.88	11.41	4.95	4.24	4.99
TiO_2	0.02	0.01	0.12	0.10	0.07	0.04	0.06	0.02	0.03	0.00	0.00	0.05
Cr_2O_3	0.00	0.06	0.01	0.00	0.05	0.06	0.06	0.00	0.03	0.00	0.19	0.13
MgO	8.48	8.50	7.86	8.27	7.71	7.37	7.26	8.21	7.65	7.38	8.91	9.64
MnO	0.00	0.02	0.03	0.00	0.00	0.01	0.11	0.00	0.00	0.03	0.02	0.00
NiO	0.00	0.03	0.00	0.04	0.03	0.04	0.00	0.00	0.00	0.03	0.00	0.00
CaO	13.74	13.90	12.63	12.97	12.41	13.03	13.62	14.50	14.50	13.17	15.32	16.28
Na_2O	6.88	6.61	7.39	7.21	7.41	7.56	6.72	6.48	6.51	7.06	6.12	5.62
K_2O	0.00	0.01	0.00	0.00	0.03	0.01	0.01	0.01	0.00	0.01	0.01	0.01
Total	99.23	99.68	99.32	98.94	99.08	100.47	99.70	99.50	99.71	99.71	99.45	100.37
Si	1.996	2.009	1.981	1.944	1.988	1.977	1.982	1.979	1.972	1.990	1.985	1.980
Al^{IV}	0.004	0.000	0.019	0.056	0.012	0.023	0.018	0.021	0.028	0.010	0.015	0.020
Al^{VI}	0.446	0.465	0.482	0.449	0.494	0.452	0.261	0.339	0.208	0.466	0.377	0.320
Fe^{2+}	0.070	0.087	0.067	0.014	0.079	0.061	0.105	0.073	0.070	0.114	0.069	0.070
Fe^{3+}	0.032	0.000	0.039	0.100	0.026	0.084	0.227	0.134	0.278	0.033	0.058	0.080
Ti	0.001	0.000	0.003	0.003	0.002	0.001	0.002	0.001	0.001	0.000	0.000	0.002
Cr	0.000	0.002	0.000	0.000	0.001	0.002	0.002	0.000	0.001	0.000	0.005	0.004
Mg	0.451	0.450	0.417	0.439	0.410	0.388	0.394	0.441	0.416	0.393	0.476	0.510
Mn	0.000	0.001	0.001	0.000	0.000	0.000	0.003	0.000	0.000	0.001	0.001	0.000
Ni	0.000	0.001	0.000	0.001	0.001	0.001	0.000	0.000	0.000	0.001	0.000	0.000
Ca	0.525	0.529	0.481	0.495	0.474	0.493	0.531	0.560	0.567	0.503	0.588	0.620
Na	0.476	0.456	0.510	0.498	0.512	0.517	0.474	0.452	0.460	0.489	0.425	0.390
K	0.000	0.000	0.000	0.000	0.001	0.000	0.000	0.000	0.000	0.000	0.000	0.000
Jd	0.445	0.461	0.475	0.419	0.489	0.441	0.256	0.328	0.200	0.459	0.371	0.314
Ae	0.032	0.000	0.039	0.094	0.026	0.082	0.223	0.130	0.267	0.033	0.057	0.079
Q	0.524	0.539	0.486	0.488	0.485	0.476	0.521	0.543	0.533	0.508	0.571	0.607

Normalized schema to 6 O. *gg* garnet glaucophanite, *r* rim, *i* clinopyroxene inclusion in garnet, *MO* high-Mg omphacite, *OM* omphacite, *AA* aegirine augite

outer 50–150 μm by the overlapping of a limited diffusion-controlled retrograde zoning (Spear 1993), especially near Grt–Omp contacts. Therefore, the retrograde effects are due to exchange reactions, spatially limited in the compositional maps and related to modification of the growth profile during the post-stage 3 evolution. A limited diffusional retrograde effect in zoning is consistent with the $T \leq 600$–625°C for the thermal peak (see below) and timescale of exhumation for these rocks. The radiating pattern may represent former microcracks which have been annealed and sealed during later stages of the Grt growth (Kurz et al. 1998). Garnet has a variable core composition both between and within samples, but the rim compositions are uniform within samples and between samples on a local scale.

In general, zoning trends of Grt in type II eclogite are very similar to those of Grt in type I eclogite (Fig. 4). However, these garnets have a less-developed bell-shaped spessartine profile, meaning that type II eclogite may be MnO-poor. They show a core-to-rim decrease of X_{Sps} and X_{Alm} (from 0.06 to 0.02 and from 0.63 to 0.55, respectively), increases of X_{Grs} and X_{Prp} (from 0.24 to 0.33 and from 0.07 to 0.13, respectively) and an overall slight decrease in X_{Fe}. X_{Prp} and X_{Alm} trends are locally reversed in the Grt rim and around Omp inclusions by retrograde Fe–Mg exchange (Spear 1993). Grt composition in glaucophanites is similar to that described for type I eclogites, and displays (not shown) an outward decrease of X_{Sps}, an increase in X_{Prp} and to a lesser extent in X_{Grs} and X_{Alm}. From core-to-rim, X_{Fe} is constant or it decreases slightly at the rim.

Clinopyroxene

Clinopyroxene composition was calculated following Morimoto (1989) and plotted on a (diopside + hedenbergite–jadeite–aegirine) Q–Jd–Ae ternary diagram. The normalization of ferric and ferrous iron was carried out using the procedure by Droop (1987). In type I eclogite, Cpx is commonly omphacite ($X_{Jd} = 0.39$–0.50, $X_{Ae} = 0.08$–0.02), with a limited, within-sample variation in composition (Fig. 6a). There is a general trend between samples of decreasing Ae content at nearly constant Q content, meaning that the controlling substitution is simply $Fe^{3+}Al_{-1}$. Some stage 3 large matrix grains in sample J74 are zoned (Fig. 6a) from omphacite cores ($X_{Jd} = 0.41$) to Mg-rich omphacite rims (until $X_{Jd} = 0.50$; Cpx-III). Stage 2 inclusions in the Omp are Qtz + Rut + Phg ± Ttn. Xenoblastic Omp inclusions

Table 4 Representative analyses of amphibole from eclogites and garnet glaucophanite

Lithology	Type I	Type I	Type I	Type I	Type I	Type I	Type I	Type I	Type I	Type I	Type II	gg	gg	gg	gg	gg
Sample	J-122	J-122	J-122	J-122	J-122	J-122	J-122	J-122	J-122	J-122	J-78	J-125	J-125	J-125	J-123	J-125
Analyses	138-c	139-i	141-i	113-r	144-r	99b-c	105-i	107-i	113-r	111-r	150-c	113-gi	123-gi	127-m	100-m	134-m
Name	Mg-Hbl	Act	Gln	Crs	Mg-Rbk	Act	Mg-Hbl	Gln	Crs	Act	Gln	Act	Act	Gln	Gln	Act
Stage	1	1	4	4	4	1	1	4	4	5	4	1	1	4	4	4, 5
SiO_2	53.13	53.58	56.94	55.29	52.41	53.34	53.23	56.11	55.29	53.53	56.60	55.73	54.87	57.50	58.06	54.28
Al_2O_3	6.51	5.96	10.59	5.97	3.34	5.54	5.33	10.94	5.97	3.19	10.74	1.58	3.06	11.84	12.00	4.17
TiO_2	0.06	0.08	0.06	0.01	0.05	0.04	0.10	0.01	0.01	0.02	0.04	0.01	0.03	0.03	0.02	0.03
Cr_2O_3	0.01	0.00	0.03	0.05	0.00	0.03	0.03	0.01	0.05	0.00	0.04	0.02	0.00	0.00	0.00	0.03
FeO	6.26	7.19	9.44	18.60	20.58	7.20	6.67	9.43	18.60	10.01	9.81	8.53	7.72	7.42	7.07	8.13
MnO	0.00	0.05	0.06	0.11	0.12	0.06	0.02	0.14	0.11	0.09	0.03	0.18	0.09	0.02	0.02	0.07
MgO	17.78	17.32	11.29	8.11	8.75	17.02	18.27	11.63	8.11	17.03	10.98	18.19	18.36	11.52	11.63	17.77
CaO	10.18	10.07	1.81	0.64	2.17	9.99	10.85	2.41	0.64	10.98	1.60	12.16	11.56	1.25	0.64	10.77
Na_2O	2.36	2.21	6.64	6.89	6.26	2.38	2.02	6.47	6.89	1.43	6.75	0.64	1.04	7.03	7.33	1.35
K_2O	0.11	0.07	0.02	0.05	0.05	0.11	0.12	0.03	0.05	0.08	0.02	0.01	0.07	0.01	0.00	0.08
Sum	96.39	96.52	96.85	95.67	93.73	95.68	96.62	97.15	95.67	96.36	96.59	97.04	96.81	96.61	96.77	96.65
Si	7.46	7.53	7.85	7.98	7.86	7.59	7.49	7.73	7.98	7.64	7.83	7.87	7.72	7.88	7.91	7.62
Al^{IV}	0.54	0.47	0.15	0.02	0.14	0.41	0.51	0.27	0.02	0.36	0.17	0.13	0.28	0.12	0.09	0.38
Al^{VI}	0.54	0.51	1.57	0.99	0.45	0.52	0.37	1.51	0.99	0.17	1.59	0.14	0.23	1.79	1.83	0.31
Ti	0.01	0.01	0.01	0.00	0.01	0.00	0.01	0.00	0.00	0.00	0.00	0.00	0.00	0.00	0.00	0.00
Cr	0.00	0.00	0.00	0.01	0.00	0.00	0.00	0.00	0.01	0.00	0.00	0.00	0.00	0.00	0.00	0.00
Fe^{3+}	0.27	0.29	0.24	0.89	1.16	0.16	0.28	0.32	0.89	0.42	0.27	0.13	0.27	0.08	0.14	0.43
Fe^{2+}	0.47	0.55	0.85	1.35	1.42	0.70	0.51	0.77	1.35	0.77	0.87	0.88	0.64	0.77	0.67	0.52
Mn	0.00	0.01	0.01	0.01	0.01	0.01	0.00	0.02	0.01	0.01	0.00	0.02	0.01	0.00	0.00	0.01
Mg	3.72	3.63	2.32	1.74	1.95	3.61	3.83	2.39	1.74	3.62	2.27	3.83	3.85	2.35	2.36	3.72
Ca	1.53	1.52	0.27	0.10	0.35	1.52	1.63	0.36	0.10	1.68	0.24	1.84	1.74	0.18	0.09	1.62
Na	0.64	0.60	1.78	1.93	1.82	0.66	0.55	1.73	1.93	0.40	1.81	0.17	0.28	1.87	1.93	0.37
K	0.02	0.01	0.00	0.01	0.01	0.02	0.02	0.00	0.01	0.01	0.00	0.00	0.01	0.00	0.00	0.01
Cat	15.19	15.13	15.05	15.03	15.18	15.20	15.21	15.09	15.03	15.09	15.06	15.02	15.04	15.05	15.03	15.00

Normalization to 23 O (IMA 1997 scheme). *gg* garnet glaucophanite, *Mg-Hbl* magnesiohornblende, *Act* actinolite, *Gln* glaucophane, *Crs* crossite, *Mg-Rbk* magnesio-riebeckite

Table 5 Representative analyses of white mica from eclogites and garnet glaucophanites

Lithology	Type I	Type I	Type I	Type I	Type I	Type I	Type II	Type II	gg	gg	gg	gg
Sample	J-74	J-74	J-74	J-74	J-74	J-74	J-78	J-78	J-122	J-122	J-122	J-122
Analyses	21-m	23-m	26-ic	27-ic	164-ig	165-ig	45-m	30-pLw	114-ig	115-ig	131-m	116-m
Stage	3	3	1, 2	1, 2	1, 2	1, 2	3	2	3	3	3, 4	3, 4
SiO_2	50.83	51.08	46.82	46.56	46.09	41.50	49.72	46.30	49.75	50.13	50.47	47.20
Al_2O_3	26.11	26.04	29.42	31.65	38.73	34.72	26.71	39.60	27.88	27.47	27.29	29.68
TiO_2	0.31	0.26	0.47	0.44	0.01	0.03	0.16	0.00	0.25	0.28	0.27	0.24
Cr_2O_3	0.00	0.00	0.00	0.01	0.04	0.04	0.04	0.00	0.03	0.00	0.00	0.03
MgO	3.69	3.99	2.56	3.11	0.10	2.05	3.36	0.11	3.86	3.81	4.12	3.42
FeO	1.42	1.23	1.09	1.19	0.81	5.17	1.87	0.57	1.34	1.21	1.63	1.38
MnO	0.00	0.00	0.00	0.03	0.00	0.02	0.03	0.00	0.00	0.00	0.01	0.02
ZnO	0.50	0.50	0.36	0.47	0.01	0.20	0.06	0.02	0.31	0.47	0.22	0.42
CaO	0.00	0.00	0.03	0.08	0.84	0.10	0.03	0.12	0.00	0.01	0.00	0.06
Na_2O	0.47	0.48	0.90	0.71	6.93	0.75	0.38	7.98	0.58	0.50	0.41	1.00
K_2O	9.98	9.93	9.49	9.47	0.22	7.51	10.03	0.04	9.78	10.01	10.12	9.45
Total	93.36	93.52	91.13	93.77	93.76	92.09	92.39	94.74	93.78	93.90	94.53	92.89
Si	6.893	6.905	6.506	6.298	5.989	5.791	6.819	5.950	6.710	6.758	6.765	6.453
Al^{IV}	1.107	1.095	1.494	1.702	2.011	2.209	1.181	2.050	1.290	1.242	1.235	1.547
Al^{VI}	3.068	3.055	3.326	3.346	3.922	3.502	3.139	3.950	3.142	3.124	3.077	3.237
Ti	0.032	0.027	0.049	0.045	0.001	0.003	0.016	0.000	0.026	0.029	0.027	0.025
Cr	0.000	0.000	0.000	0.001	0.004	0.004	0.005	0.000	0.003	0.000	0.000	0.003
Mg	0.747	0.804	0.530	0.628	0.018	0.427	0.688	0.021	0.776	0.766	0.824	0.697
Fe^{2+}	0.161	0.139	0.126	0.135	0.088	0.603	0.214	0.062	0.151	0.137	0.183	0.158
Mn	0.000	0.000	0.000	0.003	0.000	0.002	0.003	0.000	0.000	0.000	0.001	0.002
ZnO	0.050	0.050	0.037	0.047	0.001	0.020	0.006	0.002	0.031	0.047	0.021	0.042
Ca	0.000	0.000	0.005	0.011	0.116	0.015	0.004	0.017	0.000	0.001	0.000	0.009
Na	0.124	0.125	0.242	0.187	1.746	0.203	0.101	1.988	0.152	0.131	0.107	0.265
K	1.726	1.712	1.683	1.634	0.036	1.336	1.754	0.006	1.683	1.722	1.731	1.649
X_{Ms}	0.93	0.93	0.87	0.89	0.02	0.86	0.94	0.00	0.92	0.93	0.94	0.86
X_{Pg}	0.07	0.07	0.13	0.10	0.92	0.13	0.05	0.99	0.08	0.07	0.06	0.14

gg garnet glaucophanite, *m* matrix, *ic* clinopyroxene inclusion, *ig* garnet inclusion, *pLw* lawsonite pseudomorph

Table 6 Representative analyses of epidote group minerals from eclogites and garnet glaucophanites

Lithology	Type I	Type I	Type I	Type I	Type I	Type I	gg	gg	gg	gg	gg
Sample	J-74	J-74	J-74	J-74	J-74	J-74B	J-123	J-123	J-123	J-125	J-125
Analyses	35-ar	38-ar	54-ig	55-ig	17-pLw	85-pLw	86-ig	105-m	109-m	125-ig	128-m
Stage	4	4	1, 2	2	2	2	2	4, 5	3, 4	4, 5	3, 4
SiO_2	37.11	36.69	38.39	39.03	38.05	39.01	38.88	38.43	39.56	38.61	39.12
TiO_2	0.03	0.08	0.11	0.16	0.11	0.15	0.22	0.10	0.03	0.27	0.05
Al_2O_3	22.47	22.84	31.02	29.76	29.86	30.91	29.01	27.43	32.18	28.92	31.79
Fe_2O_3	13.89	13.41	2.34	3.83	4.80	3.73	5.41	7.27	1.55	5.49	1.68
MnO	0.17	0.17	0.01	0.12	0.05	0.09	0.11	0.04	0.00	0.17	0.01
MgO	0.00	0.01	0.05	0.05	0.09	0.04	0.03	0.02	0.01	0.09	0.03
CaO	23.54	23.55	24.86	24.05	24.01	24.59	24.72	24.44	25.29	24.47	25.22
Na_2O	0.00	0.01	0.01	0.01	0.00	0.03	0.03	0.03	0.02	0.01	0.02
K_2O	0.00	0.00	0.00	0.00	0.00	0.02	0.00	0.00	0.00	0.00	0.00
Cr_2O_3	0.02	0.03	0.00	0.02	0.02	0.03	0.04	0.00	0.00	0.10	0.07
Total	97.23	96.80	96.78	97.03	96.98	98.59	98.45	97.78	98.67	98.37	97.99
Si	2.991	2.969	2.978	3.026	2.965	2.980	2.997	3.003	2.998	2.987	2.990
Al	2.136	2.179	2.836	2.720	2.743	2.783	2.636	2.527	2.875	2.638	2.864
Fe^{3+}	0.842	0.817	0.137	0.224	0.281	0.214	0.314	0.427	0.088	0.320	0.097
Ti	0.002	0.005	0.007	0.009	0.007	0.009	0.013	0.006	0.002	0.016	0.003
Mg	0.000	0.001	0.005	0.006	0.010	0.005	0.003	0.003	0.001	0.011	0.003
Mn	0.012	0.012	0.000	0.008	0.004	0.006	0.007	0.003	0.000	0.011	0.001
Ca	2.033	2.042	2.066	1.998	2.004	2.013	2.041	2.046	2.054	2.028	2.065
X_{Ps}	0.28	0.27	0.05	0.08	0.09	0.07	0.01	0.14	0.03	0.11	0.03

gg garnet glaucophanite, *ar* retrograde aggregates, *m* matrix, *ig* garnet inclusion, *pLw* lawsonite pseudomorph

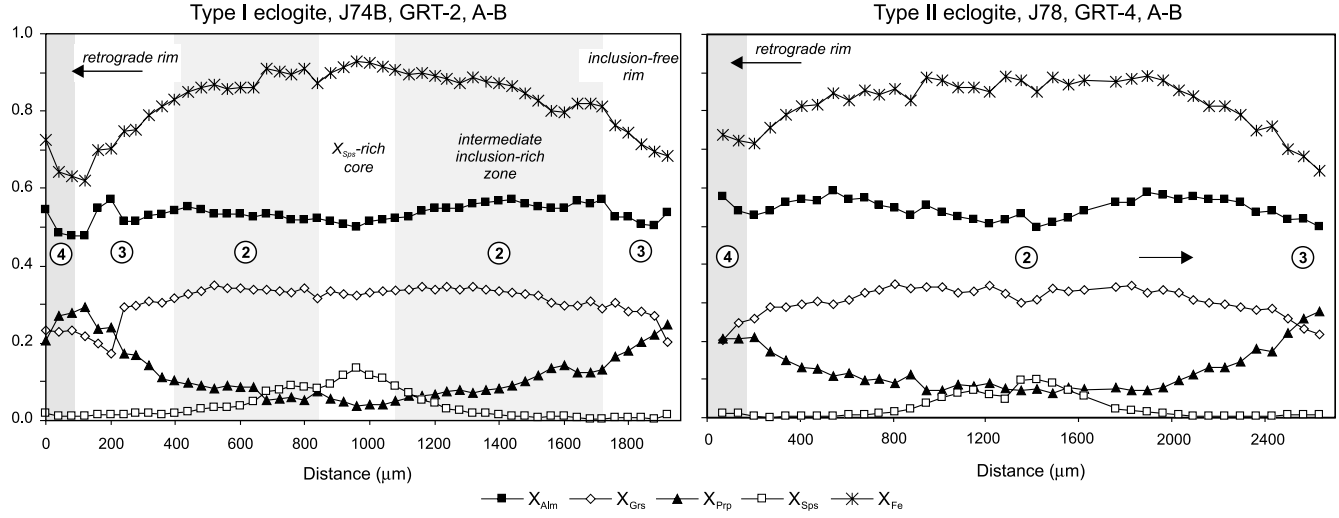

Fig. 4 Representative zoning profiles of garnet from type I and II eclogites. Encircled numbers are metamorphic evolution stages. See Fig. 2c, h for location of the compositional profiles

in stage 4 Gln are zoned from cores of $X_{Jd} = 0.42$ and $X_{Ae} = 0.04$ to rims of $X_{Jd} = 0.49$ and $X_{Ae} = 0.02$ (Fig. 2j). Stage 3 matrix Cpx in the same rock is also omphacite ($X_{Jd} = 0.41$–0.48, $X_{Ae} = 0.04$–0.09). Clinopyroxene in type II eclogite is commonly Omp ($X_{Jd} = 0.32$–0.46), but some Cpx inclusions straddle the omphacite–aegirine augite boundary (Fig. 6a). In these rocks, three compositional types of Cpx are observed (Fig. 2h): stage 1 inclusions of aegirine augite (Cpx-I: $X_{Jd} = 0.12$–0.22, $X_{Ae} = 0.27$–0.22) in Grt cores; stage 2 inclusions of omphacite (Cpx-II: $X_{Jd} = 0.26$–0.32, $X_{Ae} = 0.22$–0.15) in Grt rims and as matrix grains touching Grt; and large stage 3 Mg-rich omphacite ($X_{Jd} = 0.40$–0.46, $X_{Ae} = 0.08$–0.03) matrix nematoblasts elongated parallel to L1. Apparently, Cpx-I coexists with Lws and Cpx-II coexists with Ep + Pg pseudomorphs as inclusions in Grt grains, but never in mutual contact, different when compared to Lws + Phg + Omp + Grt assemblages of lawsonite eclogites described by Zack et al. (2004). The trend from Cpx-I to Cpx-III is to increase X_{Jd} together with a decrease in X_{Ae}, which is consistent with a prograde increase in P. In garnet glaucophanites Omp occurs only as inclusions in Grt porphyroblasts. From core-to-rim (Fig. 6a), inclusions change in compositions from Mg-rich Omp ($X_{Jd} = 0.37$–0.31, $X_{Ae} = 0.05$–0.08) to Omp ($X_{Jd} = 0.24$–0.21, $X_{Ae} = 0.04$–0.09). In sample J123, Omp

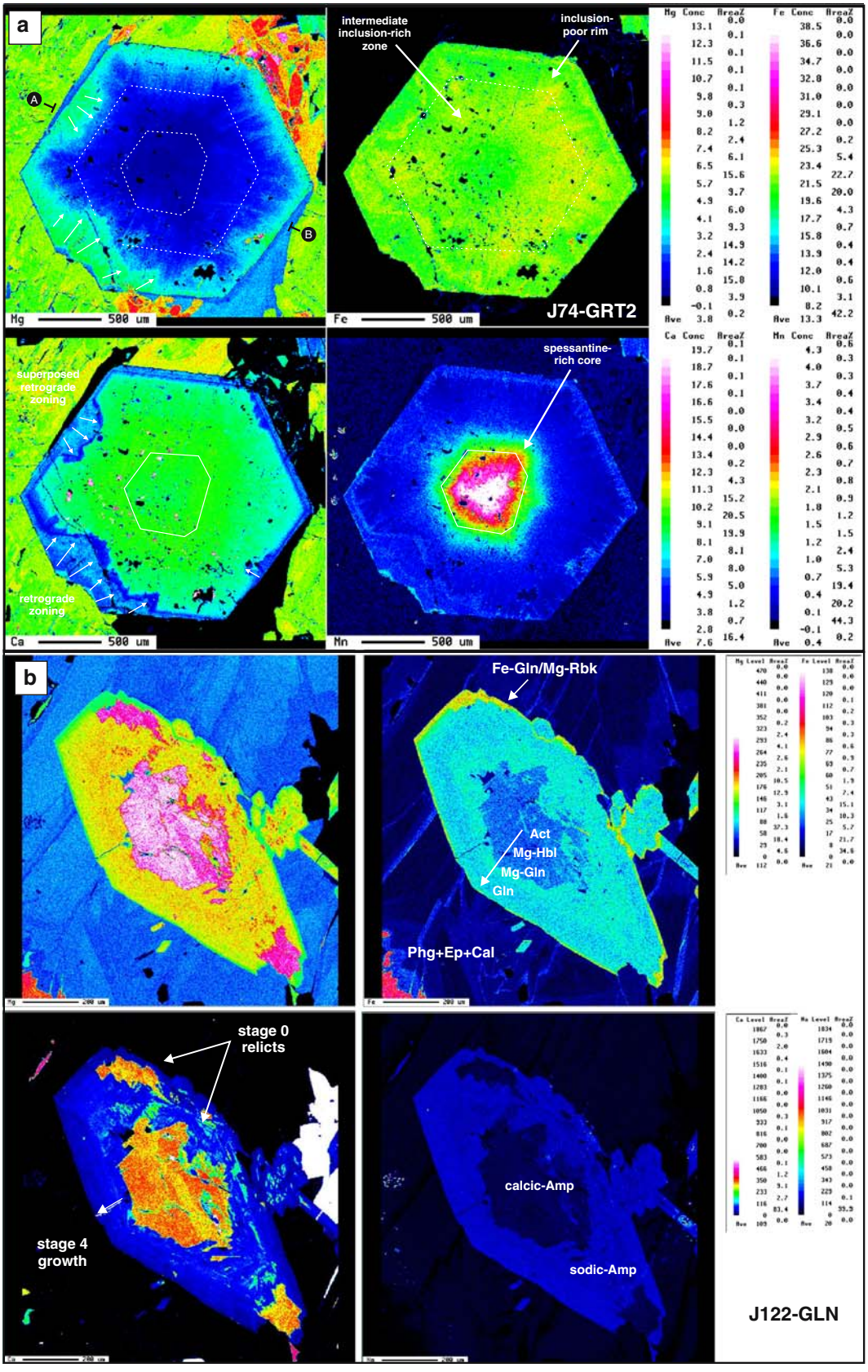

Fig. 5 **a** Element X-ray mapping images of a texturally sector-zoned garnet J74-GRT2 (Fig. 2f). **b** Element X-ray mapping images of texturally sector-zoned amphibole in sample J122

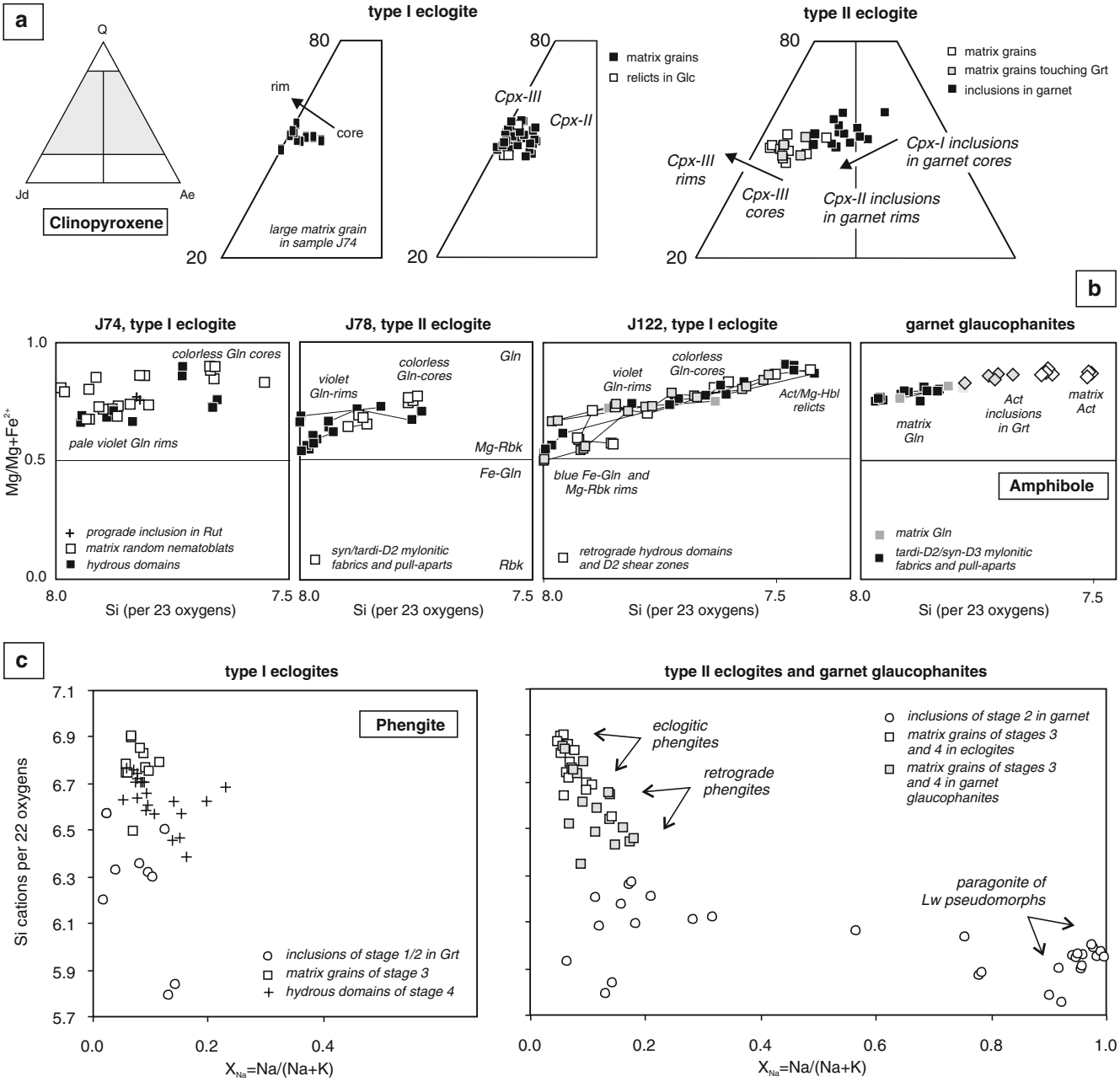

Fig. 6 **a** Ternary plots with apices jadeite, aegirine and diopside + hedenbergite illustrating the composition of clinopyroxene in eclogites. **b** Composition of the amphiboles in eclogites and garnet glaucophanite plotted in terms of the number of Si cations per 23 oxygens versus $Mg/(Mg + Fe^{2+})$. **c** Composition of the white micas plotted in terms of the number of Si cations per 22 oxygens versus $X_{Na} = Na/(Na + Ca)$

inclusions in Grt are comparatively Q-rich with $X_{Jd} = 0.38$ in the core and Q-poor with $X_{Jd} = 0.23$ in the rim.

Amphibole

In the studied rocks, sodic or calcic amphibole shows a wide range in composition, whereas calcic–sodic barroisitic amphiboles (Leake et al. 1997) are absent. Fe^{3+} content and site distribution was calculated following Droop (1987) and Schumacher (1997). Type I eclogite lacks amphibole in textural equilibrium with stage 3 eclogitic assemblage. Record of previous stages occurs as relict inclusions of Act, Mg-Hbl and rare Gln. Core-to-rim zoning in stage 4 random glaucophane ranges between 7.5–7.85 and 7.83–7.92 Si cations per 23 oxygens at 0.83–0.74 and 0.86–0.68 $X_{Mg} = Mg/(Mg + Fe^{2+})$, respectively (Fig. 6b). In these grains, $Na_{(M4)} = 1.72–1.78$ and $X_{Fe^{3+}} = Fe^{3+}/(Fe^{3+} + Al^{VI}) = 0.2–0.03$. In D2 retrograde shear zones, the stage 4 elongated amphibole is strongly zoned, commonly involving

Mg-Gln cores, zoned to Gln, and Fe-Gln or Mg-Rbk rims (Fig. 6b). This compositional evolution is recorded in core-to-rim increases of Si (7.64–8.0), Na(B) (1.58–1.93) and $X_{Fe^{3+}}$ (0.14–0.49), with a concomitant decrease of X_{Mg} (0.85–0.50). Some stage 4 Na-Amp grains contain irregular relics of Ca-Amp within the successive growth surfaces, which are in the J122 sample (Fig. 5b) Act, Act-Hbl or Mg-Hbl (Si = 7.45–7.74, $Na_{(M4)}$ = 0.32–0.48, X_{Mg} = 0.77–0.91). In the same sample, S2 matrix Gln displays a rim of stage 5 retrograde Act. In blastomylonitic type II eclogite, the amphibole subparallel to the S1–L1 eclogitic fabric is Gln (Fig. 6b). However, stage 3 Grt + Omph + Phg microdomains without stable Gln are also present. Stage 4 Gln nematoblasts have a core-to-rim trend of increasing Si (7.75–8.0), $Na_{(B)}$ (1.73–1.9) and $X_{Fe^{3+}}$ (0.18–0.02), and decreasing X_{Mg} (0.72–0.62). There is limited between- and within-sample variation in stage 4 Gln composition, which suggests formation during post-eclogite facies retrograde evolution. Three textural and compositional types of amphibole occur in the garnet glaucophanites (Fig. 6b): relic inclusions in garnet of stage 0 actinolite ($Na_{(B)}$ = 0.25–0.28); matrix colorless to violet stage 4 glaucophane ($Na_{(B)}$ = 1.74–1.82); and matrix pale green stages 4–5 actinolite ($Na_{(B)}$ = 0.36–0.39). In these rocks, coexisting Na- and Ca-Amp replaced and filled garnet pull-aparts during stage 4. Si-contents and the X_{Mg} ratio commonly are 7.7–7.8 and 0.81–0.86 in stage 1 Act; 7.53–7.64 and 0.85–0.88 in stage 4 Gln; and 7.82–7.97 and 0.75–0.81 in stage 4 Act, respectively.

White micas

Silica content in white micas ranges from 5.9 to 6.9 cations per formula unit (p.f.u.; 22 oxygens), with a moderate content of octahedrally coordinated cations. A general antithetic trend can be established for Si and Na contents from eclogites to garnet glaucophanites, with a range from 6.9 Si cations and $X_{Na} = Na/(Na + K) \approx 0.05$ to 6.5 Si cations $X_{Na} \approx 0.12$ (Fig. 6c). Three textural and compositional varieties of white mica are observed in type I eclogites: relic inclusions of phengite and paragonite of stages 1 and 2 in Grt and Omp; matrix large Phg grains of the stage 3 eclogitic assemblage; and random or subparallel to S2 Phg lepidoblasts of retrograde stage 4. For stages 1 and 2, X_{Na} and Si are 0.02–0.13 and 6.20–6.57 in Phg and 0.90–0.98 and 5.75–5.98 in Pg. In stage 3, the ranges for Phg are X_{Na} = 0.06–0.10 and Si = 6.90–6.74. Large Phg grains that touch Grt are zoned from cores of X_{Cel} = 0.38 to rim X_{Cel} = 0.26 ($X_{Cel} = [1 - X_{Ms}] \times Mg/Fe + Mg$; X_{Ms} = 4-Si p.f.u.). The core-to-rim variations of Si and X_{Na} in these Phg are 6.90–6.48 and 0.07–0.10, respectively. In retrograde stage 3 Phg Si = 6.45–6.73 and X_{Na} = 0.05–0.14, for X_{Cel} between 0.18 and 0.32. Type II eclogites contain three similar varieties of white mica (Fig. 6c): syn-D1 inclusions of Pg in Grt forming the stage 1; matrix syn-D1 to early-D2 Phg lepidoblasts of stage 3; and syn- to late-S2 Phg of the stages 4 and 5. Analyzed relic Pg displays Si and X_{Na} contents of 6.1–5.8 and 0.76–0.99. Large Phg grains of stage 3 display Si values of 6.74–6.82, for X_{Na} and X_{Cel} contents of 0.05–0.08 and 0.28–0.32. The ranges of Si, X_{Na} and X_{Cel} contents in retrograde Phg are 6.25–5.90, 0.06–0.28 and 0.02–0.06, respectively. Similarly, retrograde Phg in garnet glaucophanites has 6.60–6.88 Si cations p.f.u., X_{Na} = 0.06–0.14 and X_{Cel} = 0.23–0.34.

Epidote group minerals

The Fe^{3+} contents of epidote analyses were recalculated assuming two-site ordering with a total of eight cations per 12.5 oxygens. Clinozoisite/epidote in type I eclogite contains less Fe^{3+} than Clz/Ep in type II eclogite, which contains less Fe^{3+} than Ep in garnet glaucophanites. However, two epidote group minerals are optically and chemical recognizable in some type II eclogite and garnet glaucophanite samples (Joyce 1991) namely, low-birefringence Fe-poor Ep and Clz and strong-birefringence Fe-rich Ep (> 6.5 wt% FeOt). In type I eclogite, stage 1 and 2 Clz or Ep is present as inclusions in Grt (X_{Pis} = 0.03–0.08, $X_{Pis} = Fe^{3+}/Fe^{3+} + Al^{VI}$), as Lws pseudomorphs ($X_{Pis}$ = 0.10–0.25), and as retrograde stage 3 Ep (X_{Pis} = 0.08–0.24). Type II eclogite samples contain Ep of X_{Pis} = 0.20–0.22 as inclusions in Grt, X_{Pis} = 0.04–0.14 as Lws pseudomorphs and X_{Pis} = 0.12–0.29 in retrograde assemblages. In garnet glaucophanites, two textural types of Ep are seen: inclusions in Grt (X_{Pis} = 0.10–0.12) and large matrix nematoblasts parallel to S2. The latter are either Fe^{3+}-poor (X_{Pis} = 0.03–0.04) or Fe^{3+}-rich (X_{Pis} = 0.10–0.28).

P–T path reconstruction

Calculated equilibrium phase diagrams

The input for type I eclogite is a simplified bulk composition of sample J74, derived from the modes and electron microprobe analyses: 10 Grt ($Grs_{0.27}Prp_{0.22}Alm_{0.51}$) + 10 Omp ($Jd_{0.45}Di_{0.45}Hd_{0.10}$) + 1 Phg ($Ms_{0.55}Cel_{0.37}$ Fe-$Cel_{0.08}$) + Qtz + H_2O. In the CKNFMASH system, the computed equilibrium phase diagram for sample J74 (Fig. 7a) shows a large stability field for the assemblage Grt + Omp + Phg + Pg + Qtz (dashed area) that ranges from about 550 to 725°C and 16 to 22 kbar. The stability field for the stage 3 peak-pressure assemblage Grt + Omp + Phg + Qtz of the phengite-bearing eclogite (gray-shaded area) is separated from a kyanite-bearing eclogite region at high-*T* (625–650°C) by reactions of the type: Pg → Ky + Omp + H_2O (Liati and Seidel 1996). Under blueschist facies conditions, the equilibrium phase diagram for this rock shows a large stability field of Lws that is subdivided into garnet-bearing (lawsonite eclogite; Schmidt and Poli 1998) and garnet-absent (lawsonite-blueschist) regions at high- and low-*T*, respectively. The

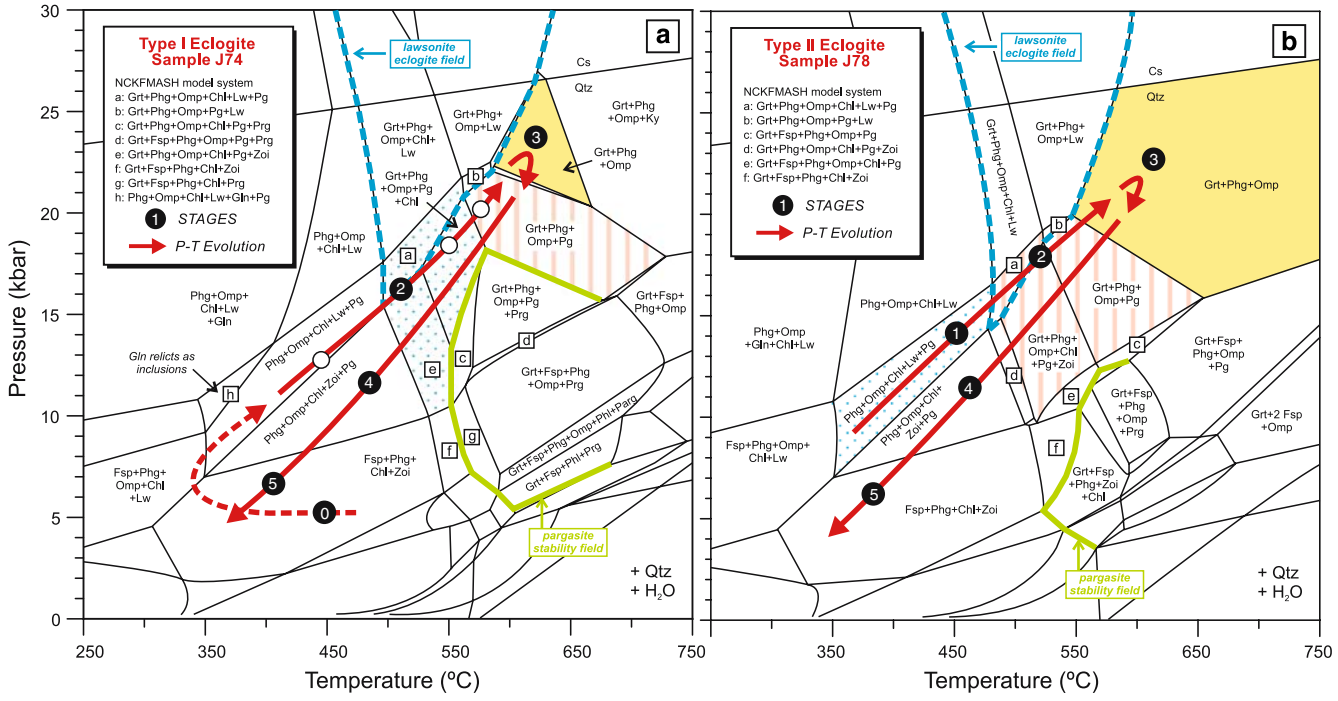

Fig. 7 Equilibrium phase diagrams calculated with DOMINO (De Capitani 1994). The *yellow shaded areas* correspond to the stability fields of the observed assemblages of stage 3 (eclogitic) peak-pressure conditions in: **a** type I eclogite and **b** type II eclogite. *Dotted* and *dashed areas* indicate *P–T* conditions of stage 1 and 2 prograde assemblages observed in thin sections. *Dashed blue line* marks the lawsonite eclogite field for these eclogite compositions. In each diagram, the *arrow* represents the reconstructed prograde and retrograde metamorphic *P–T* path

reaction that forms Grt takes place at $T = 475$–500°C at $P > 10$ kbar and has a steep negative slope in the *P–T* diagram, which corresponds with the "garnet-in" isograd described in many high-*P* blueschist terranes (Evans 1990). Between phengite-bearing eclogite and lawsonite-blueschist facies assemblages, several narrow fields occur at $T = 500$–550°C and $P < 20$ kbar (dotted area) that represent the discontinous growth of Pg and Clz and the resorbtion of Lws and Chl during increasing *P* and *T*. Probable pseudomorphs of Pg + Clz ± Qtz after Lws are preserved in the pre-D2 cores of garnets, suggesting that these stability fields were crossed during the stage 2 prograde evolution through the reaction: Lws + Gln → Pg + Clz + Chl + Qtz + H_2O (Maruyama et al. 1986). The arrow in Fig. 7a shows the interpreted prograde *P–T* path followed for type I eclogite. The mineral relicts of stage 0 metamorphism are probably stable in the low-*P* field of the greenschist facies assemblage Fsp(Ab) + Phg + Chl + Ep/Czo.

The input for type II eclogite is a simplified bulk composition of sample J78: 10 Grt ($Grs_{0.32}Prp_{0.13}Alm_{0.55}$) + 10 Omp ($Jd_{0.44}Di_{0.48}Hd_{0.08}$) + 1 Phg ($Ms_{0.59}Cel_{0.31}$ Fe-$Cel_{0.10}$) + Qtz + H_2O. Apparently, sample J78 lacks prograde Gln. In the CKNFMASH system, the peak-pressure conditions of stage 3 are reached in the field of phengite-bearing eclogite with the assemblage Grt + Omp + Phg + Qtz (yellow-shaded area) at $T > 550$°C and $P > 16$ kbar. The prograde evolution produces the following assemblages (+Qtz): Omp (Cpx-I) + Lws + Pg + Chl + Phg (stage 1; dotted area) → Grt + Omp (Cpx-II) + Lws + Pg + Chl + Phg → Grt + Omp (Cpx-II) + Pg + Ep/Clz + Phg ± Chl (stage 2; dashed area), represented by narrow fields in Fig. 7b. This *P–T* evolution (arrow) for type II eclogite is consistent with observations in thin sections.

In both types of eclogites, the retrograde conditions produced assemblages without stable garnet or barroisitic-type amphibole (syn-S2 Gln is near end-member composition). This constrains stage 4 to $T < 500$°C (without pargasite) in the Phg + Ep/Clz + Chl + Omp + Pg field, and stage 5 to the Fsp (Ab) + Phg + Chl + Ep/Clz field (Fig. 7a, b). The lack of reliable solid solution models for Na- and Ca-Amp and other phases important in the low-grade metamorphism of mafic rocks precludes an accurate low-*T* section of the diagram ($T < 450$–500°C). Additional information is obtained from mineral rim thermobarometry, as discussed below.

Mineral rim thermobarometry

The use of quantitative methods in constraining *P–T* conditions reflected by the Samaná basement complex eclogites is hampered by difficulties in inferring mineral compositions of a "stable" phase assemblage for each stage of the metamorphic evolution. Further, available thermobarometers for these rocks involve problems such as the uncertainty in Fe^{3+} content on calculated

temperatures with the Grt–Cpx Fe–Mg exchange thermometer and the lack of an accurate barometer for mafic eclogites (Spear 1993). However, the Grt + Omp + Phg + Qtz assemblage permits the use of four equilibria to estimate the *P*–*T* conditions at the stage 3 eclogitic thermal peak: the Grt–Omp thermometer (T_{EG}: Ellis and Green 1979; T_{PO}: Powell 1985; T_{KR}: Krogh 1988); the Grt–Phg Fe–Mg exchange thermometer (T_{KR}: Krogh and Råheim 1978; HF: Hynes and Forest 1988); the Si^{4+} content of phengite barometer (P_M: latest calibration of Massone 1995); and the inverse tschermak's substitution in phengite for Grt + Omp + Phg assemblages, or Grt–Omp–Phg barometer (P_{WM}: Waters and Martín 1996). For this, we used the composition of garnet, omphacite and phengite rims in textural equilibrium. In cases where no phengite was in contact with garnet, we used rims of matrix phengite with the maximum Si-content (p.f.u.).

Results obtained for rims of Grt–Omp pairs are shown in Fig. 8. As a function of the Grt–Omp geothermometer calibration used, the average calculated temperatures (±SD) at $P = 15$ kbar are 587 ± 3 (T_{EG}), 566 ± 4 (T_{PO}) and 532 ± 4°C (T_{KR}) for type I eclogites; 535 ± 2 (T_{EG}), 513 ± 2 (T_{PO}) and 486 ± 2°C (T_{KR}) for type II eclogites; and 519 ± 4 (T_{EG}), 497 ± 5 (T_{PO}) and 470 ± 5°C (T_{KR}) for omphacite inclusions and adjacent garnet pairs in garnet glaucophanites. At 15 kbar, Grt–Phg geothermometry gives average temperatures of 565 ± 3°C and 497 ± 4°C (T_{HF}) for type I and II eclogites, respectively. Minimum pressures (P_M) estimated from the composition of stage 3 phengites in type I eclogites are 14 kbar at 550°C and 15.5 kbar at 600°C. Lower pressures are obtained from similar stage 3 phengites in type II eclogites (12 kbar at 550°C, 13 kbar at 600°C) and garnet glaucophanites (11 kbar at 500°C, 12.5 kbar at 550°C). At 550°C, Grt–Cpx–Phg geobarometry gives pressures of 16.6 and 17.2 kbar (P_{WM}) for type I and II eclogites, respectively. Calculated *P*–*T* conditions fall within the stability field of stage 3 eclogitic mineral assemblages. In addition, *T* conditions are above the stability field of Lws and Gln of the blueschist facies (Evans 1990). Omphacite of composition up to Jd_{50} and Jd_{46} in type I and II eclogites, respectively, with lack of Pl in the assemblage are in accordance with $P > 12$ kbar in the range 450–550°C, defined by the position of the reaction Ab = Jd + Qtz in Fig. 8 (Holland 1983). The absence of coesite confirms $P < 25$ kbar. Estimated mineral rim equilibrium conditions are also lower than those required for the reaction Pg = Omp + Ky + H_2O, consistent with the absence of kyanite from the studied rocks. In summary, calculated *P*–*T* conditions of eclogitic stage 3 by conventional thermobarometry fall within a broad range of *P* from 12 to 23 kbar and *T* from 475 to 610°C, probably affected by retrograde Fe–Mg exchange between Grt–Omp or Grt–Phg. As discussed below, more precise estimates of *P*–*T* conditions are obtained from computed isopleths for selected end-members of relevant eclogitic phases.

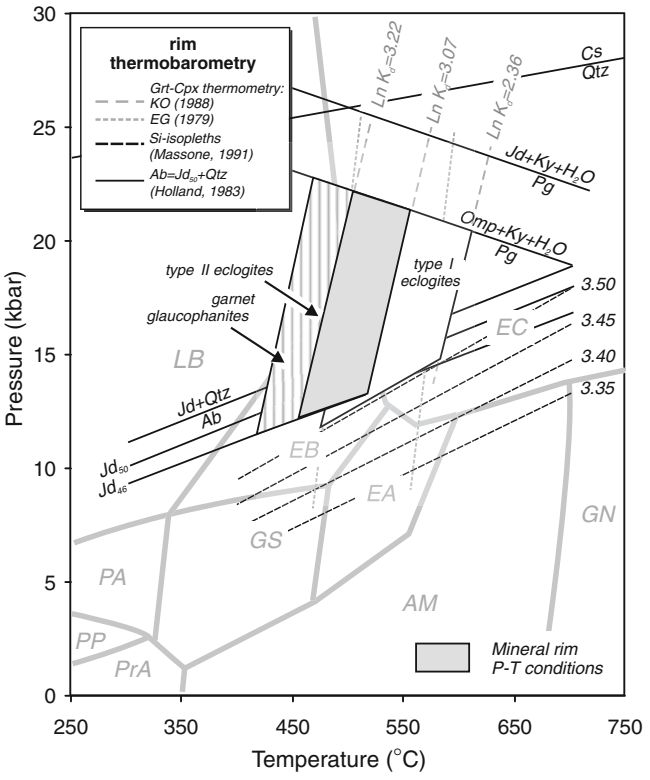

Fig. 8 Simplified *P*–*T* diagram showing the geothermobarometric results for eclogitic stage 3 using mineral rim compositions. *Gray dotted* and *strippled lines* are Ln K_d isopleths for Grt–Omp Fe–Mg exchange geothermometers of *EG* Ellis and Green (1979) and *KR* Krogh (1988; $X_{Ca} = 0.3$), respectively. *Black strippled lines* are Si-isopleths (p.f.u., 11 oxygens) for stage 3 phengite following the barometer proposed by Massone (1995). Reactions plotted in the figures are: Jd + Ky + H_2O = Pg and Omp ($X_{Jd} = 0.5$) + Ky + H_2O = Pg. Ab = Jd_{50} + Qtz reaction is the line of *P*–*T* conditions appropriate for clinopyroxene (Jd_{50}) coexisting with albite and quartz (Holland 1983). Fields of metamorphic facies compiled by Spear (1993)

Calculation of isopleths

Results of isopleth calculations with DOMINO strongly depend on bulk composition and the variance of the assemblage. Isopleths for end-members of garnet (X_{Prp}, X_{Alm} and X_{Grs}), omphacite (X_{Jd}) and phengite (X_{Cel}) were calculated in the model system CKNFMASH and are shown in Fig. 9a, b. For type I eclogite (J74), the assemblage Grt + Omp + Phg of stage 3 is stable in a restricted *P*–*T* field, in which all phase components of Grt, Omp and Phg display a narrow spread of isopleths, consistent with these three phases having undergone significant compositional changes (Fig. 9a). The circle represents the conditions of re-equilibration during peak-pressure conditions that is a region of intersection of isopleths in agreement with the real measurements (Table 7). The obtained *P*–*T* conditions for stage 3 are of 625°C and 24 kbar. On the other hand, in the Grt + Lws and Grt + Pg + Zoi stability fields, Grt and Phg isopleths are narrowly spaced, suggesting drastic

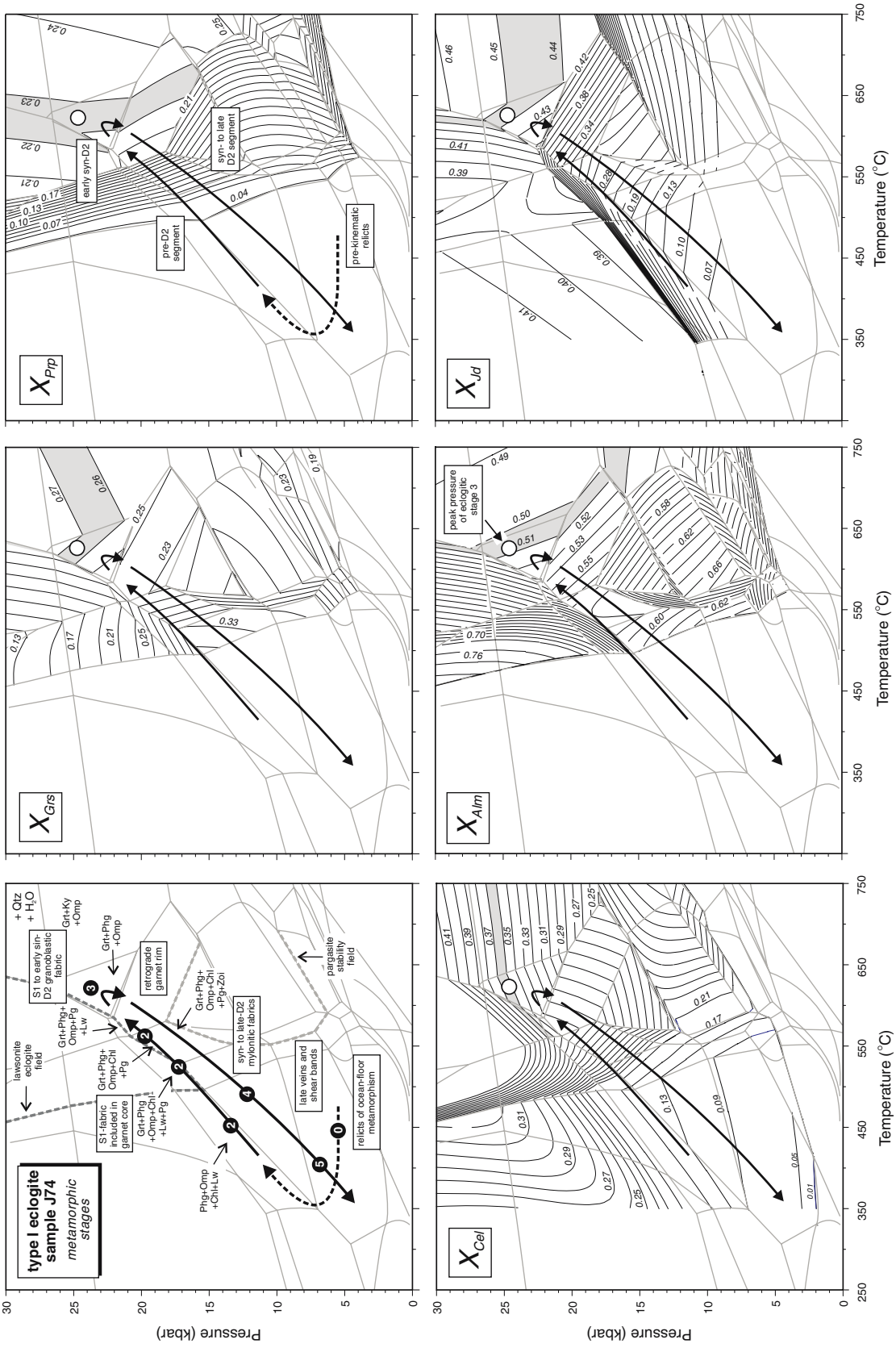

Fig. 9 Isopleths for X_{Prp}, X_{Alm}, X_{Grs}, X_{Jd} and X_{Cel} (*black lines*) computed for two samples of type I (sample J74) and type II (sample J78; Fig. 9, continuation) eclogites with the program DOMINO (De Capitani 1994). The *gray lines* outline the calculated stability fields as shown in Fig. 6. For type I and II eclogite are in this case around the 24 kbar at 625°C (J74) and 23 kbar at 610°C (J78), respectively (see also Table 7)

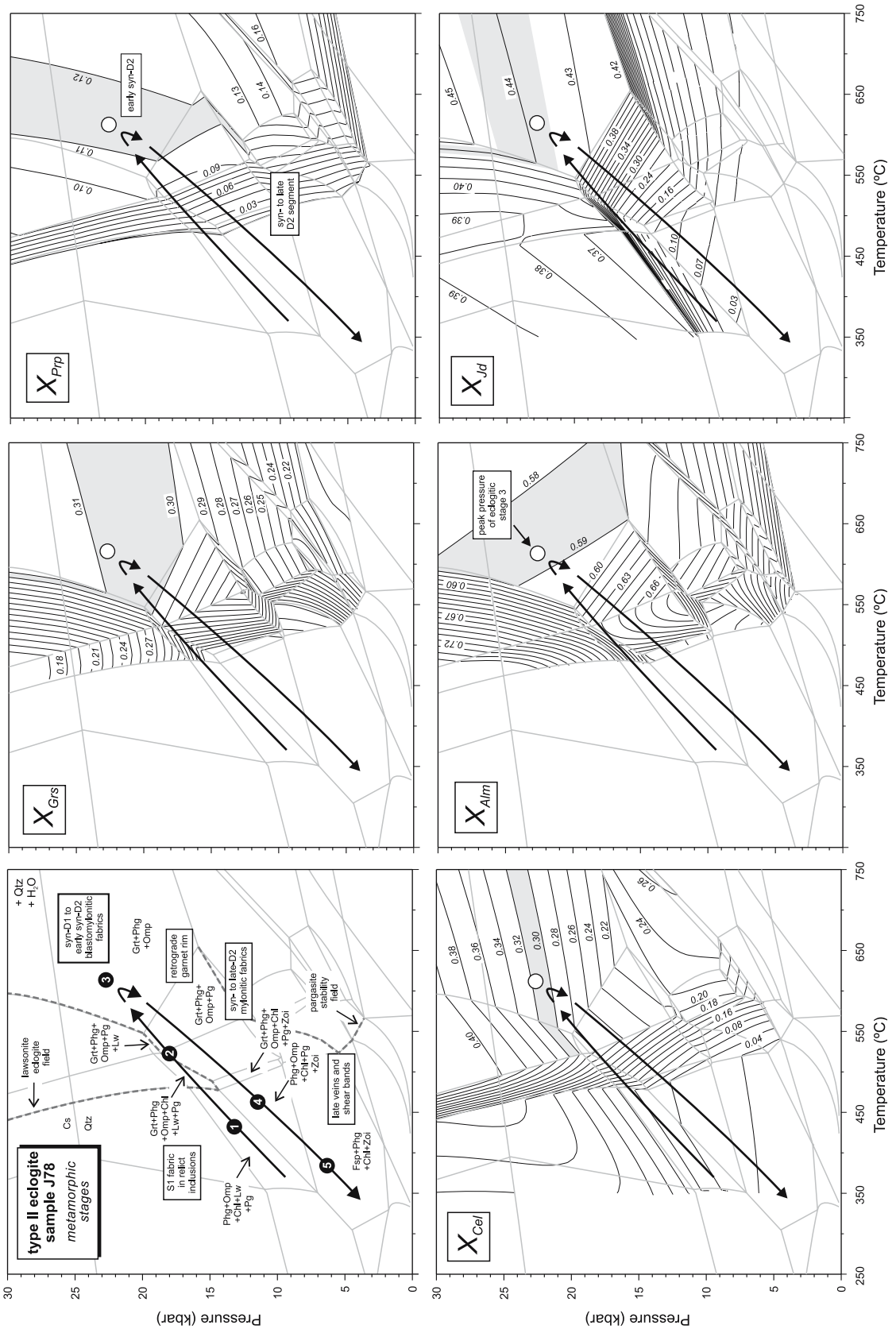
type II eclogite
sample J78
metamorphic
stages
lawsonite
eclogite
field
Cs
Qtz
+ Qtz
+ H2O
S1 fabric
in relict
inclusions
Grt+Phg
+Omp+Chl
+Lw+Pg
Phg+Omp
+Chl+Lw
+Pg
Grt+Phg+
Omp+Pg
+Lw
syn-D1 to
early syn-D2
blastomylonitic
fabrics
Grt+Phg
+Omp
retrograde
garnet rim
Grt+Phg+
Omp+Pg
syn- to late-D2
mylonitic fabrics
Grt+Phg+
Omp+Chl
+Pg+Zoi
Phg+Omp
+Chl+Pg
+Zoi
late veins and
shear bands
pargasite
stability
field
Fsp+Phg
+Chl+Zoi
Pressure (kbar)
Temperature (ºC)
X Prp
early syn-D2
syn- to late
D2 segment
X Grs
X Alm
peak pressure
of eclogitic
stage 3
X Jd
X Cel

Fig. 9 (Contd.)

Table 7 *P–T* estimates in eclogites from the Samaná metamorphic complex

Sample	Paragenesis (observed)	X_{Alm}	X_{Prp}	X_{Grs}	X_{Jd}	X_{Cel}	Garnet
(a) Measured							
J74	Grt + Omp + Phg + Qtz + Rut	0.507	0.221	0.272	0.449	0.367	rim
J78	Grt + Omp + Phg + Qtz + Rut	0.570	0.120	0.310	0.458	0.312	rim
J71	Grt + Omp + Phg + Qtz + Chl + Pg + Lw?	0.648	0.038	0.315	0.359	0.022	core
J71	Grt + Omp + Phg + Qtz + Chl + Pg + Lw?	0.633	0.055	0.310	0.310	0.286	interm
J71	Grt + Omp + Phg + Qtz	0.628	0.110	0.258	0.442	0.287	rim

Sample	$P/T^{(*)}$	Paragenesis (calculated)	X_{Alm}	X_{Prp}	X_{Grs}	X_{Jd}	X_{Cel}
(b) Calculated with DOMINO							
J74	24/625	Grt + Omp + Phg + Qtz + Rut stage 3 eclogitic peak	0.508	0.235	0.255	0.440	0.354
J74	16.5/520	Grt + Omp + Phg + Chl + Pg + Zoi prograde *P–T* point (+ Qtz + Rut)	0.580	0.080	0.339	0.238	0.236
J78	23/610	Grt + Omp + Phg + Qtz + Rut stage 3 eclogitic peak	0.598	0.114	0.287	0.436	0.307
J71	16.5/475	Grt + Omp + Phg + Lw + Chl garnet core (+ Qtz + Pg + Rut)	0.654	0.025	0.302	0.352	0.098
J71	17/490	Grt + Omp + Phg + Lw + Chl garnet intermediate (+ Qtz + Pg + Rut)	0.668	0.055	0.292	0.345	0.242
J71	20/560	Grt + Omp + Phg + Pg garnet rim (+ Qtz + Rut)	0.607	0.123	0.269	0.439	0.292
J71	21/580	Grt + Omp + Phg eclogitic peak (+ Qtz + Rut)	0.589	0.132	0.278	0.489	0.287

(a) Eclogitic parageneses observed in the thin section of the three samples, and measured end-member compositions of omphacite, garnet and phengite. (b) Calculated parageneses with the DOMINO program (De Capitani 1994) in the NaCaKFMASH system (*P–T–X* values) and the corresponding calculated end-member compositions of omphacite, garnet and phengite at the *P–T* conditions of the samples. X_{Alm} = Fe + Mn/(Fe + Mn + Mg + Ca). *P–T–X* values calculated for three points in sample J71 are for modeling a segment of the prograde *P–T* path assuming the stability of an initial assemblage of lawsonite eclogite. (*) Pressure in kbar, temperature in °C

changes in the proportions of these components (growth) in a narrow *P–T* interval. For type II eclogite (J78), however, the composition of Grt and Omp within the large stability field of the observed eclogitic assemblage Grt + Phg + Omp is almost constant, because all of the components of these two phases display isopleths widely spread over a large *P–T* range (Fig. 9b). This is probably due to the lack of Na-rich phases other than Omp. For the eclogitic peak, the estimated $T = 610$°C and $P = 23$ kbar. In a similar type II eclogite (J71 sample), the occurence of Omp, Phg and Lws inclusions in the Grt has permitted us to calculate *P–T* points relative to the core, intermediate and garnet rim, assuming that lawsonite eclogite was a prograde stable assemblage (reported by Zack et al. 2004). The obtained conditions (Table 7) record a prograde *P–T* segment from stage 2, crossing the low-*P* field of lawsonite eclogite, to stage 3 phengite eclogite.

Modeling of the *P–T* path in the CKNFMASH system

The modeled *P–T* paths for type I and II eclogites (Fig. 9a, b) can be divided into four segments where distinctive changes in mineralogy occur.

1. Pre-kinematic relicts of Ca-Amp (stage 0) are characteristic of the transition between the greenschist and lower amphibolite facies, and consistent with ocean floor mid-*T*/low-*P* metamorphism. Alternatively, the very low Ca content of amphibole can indicate relicts of prograde high-*P* greenschist facies.
2. The pre-D2 segment in type I eclogite and the S1 fabric relicts in type II eclogite belong to the Lws and Gln stability field. This *P–T* segment defines a prograde path from about 350 to 400°C and 8 to 12 kbar to the lawsonite-blueschists facies conditions, in the garnet-free first (stage 1) and the garnet-bearing next (stage 2). Onset of Grt growth where Lws + Omp was stable (+ Phg + Pg + Chl) represents crossing a field of low-*P* lawsonite eclogite facies. With increasing temperature Zoi and Pg form at the expense of Lws. In type I and II eclogites, the modeled compositional changes establish a X_{Prp} increase and a X_{Grs} decrease, comparable in absolute amounts with the zoning observed in the pre-D2 Grt cores. X_{Cel} in Phg is nearly constant (0.14–0.18) in the garnet-free lawsonite field is due to the fact that the *P–T* path is at a small angle to the slope of the isopleths, and increases strongly (from 0.20 to 0.34, type I; from 0.10 to 0.26, type II) in the garnet-blueschist facies. In the Cpx, X_{Jd} increases from 0.14 to 0.34 in type I and from 0.12 to 0.40 in type II eclogites.
3. The *P–T* segment of the stage 3, located in the phengite-bearing eclogitic field (± Pg), records rising *P* and *T* to the thermal peak (22–24 kbar at 610–630°C). This segment corresponds to the development of the inclusion-free garnet rim over the S1 fabric in type I eclogite and the early syn-S2 blastomylonitic fabric in type II eclogite. In both types, the calculated X_{Prp} increases slightly, X_{Grs} remains constant and X_{Alm} decreases. These trends are consistent with the measured compositional profiles of the syn-D2 garnet rims, away from the retrogressed outer rims. X_{Jd} strongly increases to 0.43–0.45 isopleths in both types of eclogites. X_{Cel} increases slightly in the high-*P* end of the segment (0.35–0.37, type I; 0.30–0.32, type II), as result of the parallelism of the isopleths and the *P–T* path.

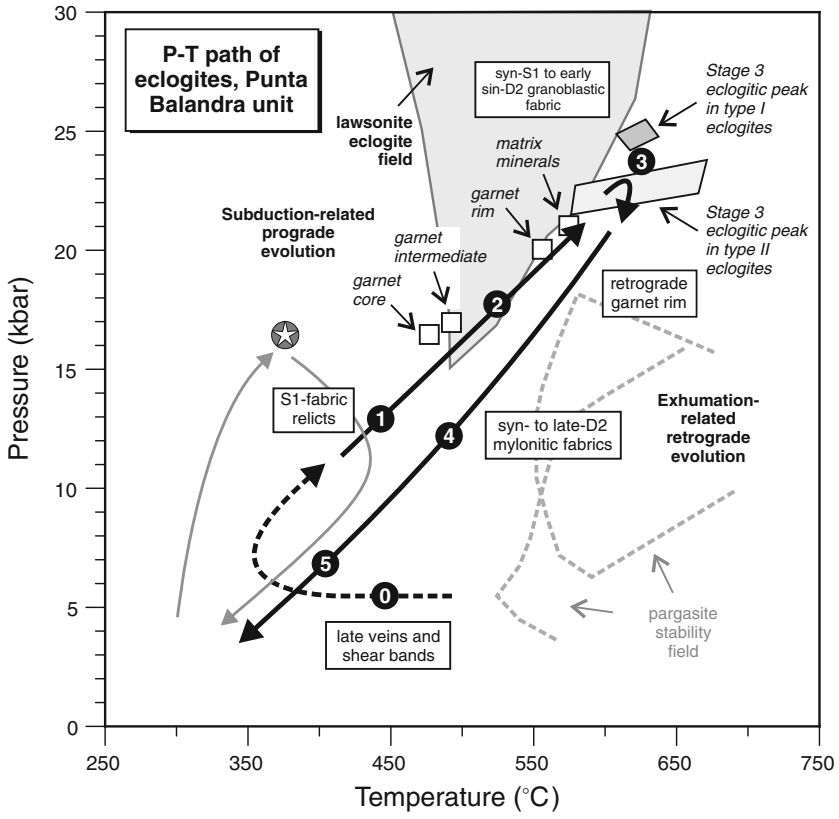

Fig. 10 *P–T* path for studied eclogites of the Punta Balandra unit of Samaná complex. *Rectangular areas* indicate DOMINO thermobarometric results for metamorphic stages 2 and 3, including prograde *P–T–X* values for J71 sample (with a probable initial lawsonite eclogite stage), and number in *circles* are the defined metamorphic stages. *Squares* are *P–T–X* values calculated in sample J71. *Boxes* are DOMINO results. *Star*: *P–T* path deduced for the lawsonite eclogite sample of Zack et al. (2004)

4. The syn- to late-D2 segment, located in the Lws-free field, is characterized by decompression and cooling, from the eclogitic peak conditions to epidote-blueschist (8–12 kbar at 400–500°C; stage 4) and greenschist facies conditions (4–8 kbar at 400–350°C; stage 5). The derived retrograde *P–T* path is subparallel to the prograde *P–T* evolution (i.e., indicates cooling during the exhumation of the eclogites), which explains the lack of barroisitic Na–Ca-Amp in all Punta Balandra unit rocks. The calculated X_{Alm}, X_{Grs} and X_{Fe} increase and X_{Jd} decrease (from 0.44 to 0.18) are consistent with reversal in the compositional trends in Grt rims by Fe–Mg exchange with adjacent Omp. Along the retrograde *P–T* path, phengite adapts its composition continuously to the changing equilibrium conditions. This results in a strong zonation in Si-content from core-to-rim and in separate grains. This *P* (and *T*) dependence of Phg composition can be used for *P–T* estimations. In Fig. 9, isopleths of aluminoceladonite content (X_{Cel}) are plotted, based on the phengite solid solution model of Massonne and Szpurka (1997). The Si-content zonation in Phg of J74 sample from Si≈3.45 p.f.u. ($X_{Cel}=0.36$) in the core to Si≈3.18 ($X_{Cel}=0.23$) in the rim reflects a *P* decrease from 24 to ~13 kbar at 550–600°C. Si-content in Phg for the J78 sample ranges from Si≈3.42 p.f.u. ($X_{Cel}=0.32$) in the core to Si≈3.26 ($X_{Cel}=0.25$) in the rim that reflects a *P* decrease from 22 to ~14 kbar at 550–600°C. It should be noted that the lowest-*T* part of this retrograde *P–T* path ($P<7$–10 kbar) is constrained by the late growth of Mg-Rbk at the rim of Gln, Act and the late greenschist facies S2 shear fabrics.

Conclusions

Eclogites and garnet glaucophanites from the Punta Balandra unit of the Samaná basement complex have undergone a clockwise metamorphic *P–T* path (Fig. 10). Two textural types of eclogites with coeval evolutions of mineral assemblages relative to slightly different gabbroic protoliths are recognized, resulting in peak metamorphism at similar eclogite facies conditions. The prograde path evolved from garnet-free lawsonite-blueschist facies to garnet-bearing lawsonite-blueschist facies to eclogite facies conditions, with a probable intermediate stage of low-*P* lawsonite eclogite (if Lw + Omp + Grt assemblage was stable). The subsequent retrograde *P–T* path entered the epidote-blueschist (garnet-free) facies, ended within the greenschist facies. The retrograde path is similar to the prograde path at low-*P* and is typical of a Franciscan-type metamorphism that Ernst (1988) suggested occurs in intraoceanic subduction zones. Franciscan-style subduction settings are characterized by relatively low geothermal gradients indicative of refrigeration during subduction zone-parallel ascent and exhumation of these rocks.

Gonçalves et al. (2000) describe the Samaná basement complex as a transpressive accretionary wedge built on the forearc area of the Caribbean island-arc system. Accretionary wedges are favorable locations for the detachment of slices of "normal" oceanic crust from the subducting plate, metamorphosed to blueschist and eclogite facies conditions at great depths. These slices subsequently are being rapidly uplifted towards the surface by subduction channeling (Cloos and Shreve 1988), extensional underplating (Platt 1993) or serpentinite diapirism (Guillot et al. 2000). Escuder-Viruete and Pérez-Estaún (2004) interpret the Samaná basement complex as an imbricate stack of discrete tectonic units formed in an accretionary complex below a forearc basin, deformed by a sinistral strike-slip and reverse faults tectonics associated with the Neogene movement of the Septentrional fault zone. The intensity of ductile deformation and the development of non-coaxial metamorphic fabrics at different metamorphic conditions vary from each thrust slab, but the kinematic indicators consistently indicated a top-to-the E and ENE shear sense. Thus, Samaná basement complex eclogites and garnet glaucophanites formed by the WSW/W-directed subduction of Atlantic lithosphere beneath the Caribbean plate. Thrust stacking and wrenching of different tectonic slices can provide a mechanism for late stage exhumation and cooling due to underplating and explain the preservation of high-pressure assemblages.

The tectonometamorphic history of the Punta Balandra unit can be established with the aid of geochronological data. Imprecise Sm-Nd isochron ages of 84 ± 22 Ma (Joyce 1991) and 86 ± 47 Ma (Grt–Omp–whole rock; Escuder-Viruete et al. 2004) suggest that the eclogitic stage 3 formed during the final stages of subduction of the protoliths during the Upper Cretaceous to Lower Eocene. The late D2 deformation formed a blueschist facies mylonitic S2–L2 fabric and was contemporaneous with top-to-the ENE/E emplacement of the eclogite-bearing Punta Balandra unit onto other high-*P* Samaná basement complex units within a subduction zone (Escuder-Viruete and Pérez-Estaún 2004). Phengite K-Ar ages of 38 ± 2 Ma obtained by Joyce and Aronson (1987) and phengite $^{40}Ar/^{39}Ar$ ages that range from Eocene to late Oligocene obtained by Catlos and Sorensen (2003) in eclogite blocks probably record retrogression and uplift related to emplacement of the unit. Recently, Late Eocene to Early Oligocene $^{40}Ar/^{39}Ar$ plateau cooling ages are obtained from phengite in banded eclogite (35.65 ± 0.73 Ma) and foliated (S2) garnet glaucophanite (33.68 ± 0.47 Ma) by Escuder-Viruete et al. (2004), and are attributed to the regional exhumation of the Punta Balandra unit triggered by the initial oblique collision of the Bahama Platform beneath the Caribbean arc in Hispaniola. These ages are consistent with the Middle Eocene folding and uplift of the overlying forearc basin (De Zoeten and Mann 1999), which is filled by Paleocene to Early Eocene deep-marine sediments of Imbert and Los Hidalgos Formations. Regional uplift produced clasts of high-*P* rocks and the deposition from Late Eocene to Early Miocene of a several kilometers thick turbiditic succession of the Mamey Group, within a W-NW-trending elongate basin. This folding and uplift event also coincides with the cessation of most subduction-related magmatism in northern Hispaniola.

Acknowledgments This study received financial aid from MCYT projects BTE-2002-00326 and CGL2005-02162/BTE. J. Lewis and G. Draper are thanked for the initial field-work and previous review (GD) of the manuscript. Also, we are grateful for the support, field-assistance and geological discussions of numerous colleagues of the IGME-BRGM-INYPSA group, devoted to the geological mapping of the Dominican Republic (SYSMIN project). We thank J. González del Tánago and A. Larios from the CAI Lluís Brú of the UCM for the kind help with elemental X-ray mapping of minerals. A. Indares is thanked for the very helpful and rigorous previous review. We also express our thanks to P. O'Brien and A. Willner for constructive critical comments and careful review of the manuscript.

References

Berman RG (1988) Internally-consistent thermodynamic data for minerals in the system Na_2O–K_2O–CaO–MgO–FeO–Fe_2O_3–Al_2O_3–SiO_2–TiO_2–H_2O–CO_2. J Petrol 29:445–522

Berman RG (1990) Mixing properties of Ca–Mg–Fe–Mn garnets. Am Mineral 75:328–344

Carswell DA (1990) Eclogites and the eclogite facies: definitions and classification. In: Carswell DA (ed) Eclogite facies rocks. Blackie, London, pp 1–13

Catlos EJ, Sorensen SS (2003) Phengite-based chronology of K- and Na-rich fluid flow in two paleosubduction zones. Science 299:92–95

Chatterjee ND, Froese E (1975) A thermodynamic study of the pseudobinary join muscovite–paragonite in the system $KAlSi_3O_8$–$NaAlSi_3O_8$–Al_2O_3–SiO_2–H_2O. Am Mineral 60:985–993

Cloos M, Shreve RL (1988) Subduction-channel model of prism accretion, melange formation, sediment subduction, and subduction erosion at convergent plate margins: 1. Background and description. Pure Appl Geophys 128:455–499

De Capitani C (1994) Gleichgewichts-Phasendiagramme: Theorie und Software. Beihefte zum European Journal of Mineralogy, 72. Jauhrestagung der Deutschen Mineralogischen Gesellschaft 6:48

De Zoeten R, Mann P (1999) Cenozoic El Mamey Group of northern Hispaniola: a sedimentary record of subduction, collisional and strike-slip events within the North America–Caribbean plate boundary zone. In: Mann P (ed) Caribbean basins. Sedimentary basins of the word 4, pp 247–286

Dolan J, Mullins H, Wald D (1998) Active tectonics of the north-central Caribbean region: oblique collision, strain partitioning and opposing slabs. In: Dolan J, Mann P (eds) Active strike-slip and collisional tectonics of the Northern Caribbean plate boundary zone in Hispaniola. Geol Soc Am Spec Pap 326:1–61

Draper G, Nagle F (1991) Geology, structure and tectonic development of the Río San Juan Complex, northern Dominican Republic. In: Mann P, Draper G, Lewis J (eds) Geologic and tectonic development of the North America–Caribbean plate boundary zone in Hispaniola. Geol Soc Am Spec Pap 262:77–95

Droop GTR (1987) A general equation for estimating Fe3+ concentrations in ferromagnesian silicates and oxides from microprobe analysis using stoichiometric criteria. Mineral Mag 51(361):431–435

Ellis DJ, Green DH (1979) An experimental study of the effect of Ca upon garnet-clinopyroxene Fe–Mg exchange equilibria. Contrib Mineral Petrol 71:13–22

Ernst WG (1988) Tectonic history of subduction zones inferred from retrograde blueschist P-T paths. Geology 16:1081–1084

Escuder-Viruete J, Pérez-Estaún A (2004) Trayectoria metamórfica P–T relacionada con subducción en eclogitas del Complejo de Basamento de Samaná, Cordillera Septentrional, República Dominicana. Geo-Temas 6(1):37–40

Escuder-Viruete J, Iriondo A, Premo WR, Pérez-Estaún A (2004) Subduction, collision and exhumation events within Caribbean–North America plate boundary zone: geochronological constraints from eclogites and blueschists of the Samaná Peninsula complex, Northern Hispaniola. Geoph Res Abs 6:06964

Evans BW (1990) Phase relations of epidote-blueschists. Lithos 25:3–23

Fuhrman ML, Lindsley DH (1988) Ternary feldspar modeling and thermometry. Am Mineral 73:201–215

Gonçalves Ph, Guillot S, Lardeaux JM, Nicollet C, Mercier de Lépinay B (2000) Thrusting and sinistral wrenching in a pre-Eocene HP-LT Caribbean accretionary wedge (Samaná Peninsula, Dominican Republic). Geodinamica Acta 13:119–132

Guillot S, Hattori KH, de Sigoyer J (2000) Mantle wedge serpentinization and exhumation of eclogites: insights from eastern Ladakh, northwest Himalaya. Geology 28(3):199–202

Holland TJB (1983) The experimental determination of activities in disordered and short-range ordered jadeite clinopyroxenes. Contrib Mineral Petrol 82:214–220

Hynes A, Forest RC (1988) Empirical garnet-muscovite geothermometry in low-grade metapelites, Selwyn Range (Canadian Rockies). J Metamorphol Geol 6:297–309

Joyce J (1991) Blueschist metamorphism and deformation on the Samaná Peninsula: a record of subduction and collision in the Greater Antilles. In: Mann P, Draper G, Lewis J (eds) Tectonic development of the North America–Caribbean plate boundary zone in Hispaniola. Geol Soc Am Spec Pap 262:47–75

Joyce J, Aronson J (1987) K-Ar ages for blueschist metamorphism on the Samaná Peninsula, Dominican Republic. In: Transaction of 10th Caribbean Geological Conference, Cartagena, Colombia, pp 454–458

Konrad-Schmolke M, Handy MRBJ, O'Brien PJ (2005) Thermodynamic modelling of diffusion-controlled garnet growth. Contrib Mineral Petrol 16:181–195

Kretz R (1983) Symbols for rock-forming minerals. Am Mineral 68:277–279

Krogh EJ (1988) The garnet-clinopyroxene Fe–Mg geothermometer—a reinterpretation of existing experimental data. Contrib Mineral Petrol 99:44–48

Krogh EJ, Råheim A (1978) Temperature and pressure dependence of Fe–Mg partitioning between garnet and phengite, with particular reference to eclogites. Contrib Mineral Petrol 66:75–80

Kurz W, Neubager F, Dachs E (1998) Eclogite meso- ad microfabrics: implications for the burial and exhumation history of eclogites in the Tauern Window (Eastern Alps) from P-T-d paths. Tectonophysics 285:183–209

Leake BE, Woolley AR, Arps CES, Birch WD, Gilbert MC, Grice JD, Hawthorne FC, Kato A, Kisch HJ, Krivovichev VG, Linthout K, Laird J, Mandarino JA, Maresch WV, Nickel EH, Rock NMS, Schumacher JC, Smith DC, Stephenson NCN, Ungaretti L, Whittaker EJW, Youzhi G (1997) Nomenclature of amphiboles: report of the subcommittee on amphiboles of the International Mineralogical Association, Commission on New Minerals and Mineral Names. Am Mineral 83:1019–1037

Liati A, Seidel E (1996) Metamorphic evolution and geochemistry of kyanite eclogites in Rhodope, northern Greece. Contrib Mineral Petrol 123:293–307

Mäder UK, Berman RG (1992) Amphibole thermo-barometry: a thermodynamic approach. Current Research, Geological Survey Canada Paper 92-1E, pp 393–400

Mäder UK, Percival JA, Berman RG (1994) Thermo-barometry of garnet clinopyroxene–hornblende granulites from the Kapuskasing structural zone. Can J Earth Sci 31:1134–1145

Mann P (1999) Caribbean sedimentary basins: classification and tectonic setting from jurassic to present. In: Mann P (ed) Caribbean basins. Sedimentary basins of the word 4, pp 3–31

Mann P, Draper G, Lewis JF (1991) An overview of the geologic and tectonic development of Española. In: Mann P, Draper G, Lewis JF (eds) Geologic and tectonic development of the North America–Caribbean plate boundary in Española. Geol Soc Am Spec Pap 262:1–28

Maruyama S, Cho M, Liou JG (1986) Experimental investigations of blueschist–greenchist transition equilibria; pressure dependence of Al_2O_3 contents in sodic amphiboles; a new geobarometer. In: Evans BW, Brown EH (eds) Blueschist and eclogites. Geol Soc Am Mem 164:1–16

Massone HJ (1995) Experimental and petrogenetic study of UHPM. In: Coleman RG, Wang X (eds) Ultrahigh pressure metamorphism. Cambridge University Press, Cambridge, pp 33–95

Massonne HJ, Szpurka Z (1997) Thermodynamic properties of white micas on the basis of high-pressure experiments in the systems K_2O–MgO–Al_2O_3–SiO_2–H_2O and K_2O–FeO–Al_2O_3–SiO_2–H_2O. Lithos 41:229–250

Meyre C, de Capitani C, Partzsch JH (1997) A ternary solid solution model for omphacite and its application to geothermobarometry of eclogites from the Middle Adula nappe (Central Alps, Switzerland). J Metamorphol Geol 15:687–700

Morimoto N (1989) Subcommittee on Pyroxenes, Nomenclature of pyroxenes. Can Mineral 27:143–156

Nagle F (1974) Blueschist, eclogite, paired metamorphic belts, and the early tectonic history of Hispaniola. Geol Soc Am Bull 85:1461–1466

Pindell JL, Draper G (1991) Stratigraphy and geological history of the Puerto Plata area, northern Dominican Republic. Geol Soc Am Spec Pap 262:97–114

Platt JP (1993) Exhumation of high-pressure rocks: a review of concepts and processes. Terra Nova 5:119–133

Powell R (1985) Regression diagnostics and robust regression in geothermometer/geobarometer calibration: the garnet–clinopyroxene geothermometer revisited. J Metamorphol Geol 3:231–243

Schmidt MW, Poli S (1998) Experimentally based water budgets for dehydrating slabs and consequences for arc magma generation. Earth Planet Sci Lett 163:361–379

Schumacher JC (1997) Apendix 2. The estimation of the proportion of ferric iron in the electronic-microprobe analysis of amphiboles. Can Mineral 35:238–246

Spear FS (1993) Metamorphic phase equilibria and pressure–temperature–time paths. Mineral Society of America Monograph, Washington, DC

Waters D, Martín M (1996) Garnet–clinopyroxene–phengite barometry (http://www.earth.ox.ac.uk/~davewa/research/ecbarcal.html)

Willner AP (2005) Pressure_temperature evolution of a Late Palaeozoic paired metamorphic belt in North-Central Chile (34°–35°30′S). J Petrol 46:1805–1833

Zack T, Rivers T, Brumm R, Kronz A (2004) Cold subduction of oceanic crust: implications from a lawsonite eclogite from the Dominican Republic. Eur J Mineral 16:909–916